How Do Outer Spiral Rainbands Affect Tropical Cyclone Structure and Intensity?*

YUQING WANG

International Pacific Research Center, and Department of Meteorology, School of Ocean and Earth Science and Technology, University of Hawaii at Manoa, Honolulu, Hawaii

(Manuscript received 15 January 2008, in final form 13 October 2008)

ABSTRACT

A long-standing issue on how outer spiral rainbands affect the structure and intensity of tropical cyclones is studied through a series of numerical experiments using the cloud-resolving tropical cyclone model TCM4. Because diabatic heating due to phase changes is the main driving force of outer spiral rainbands, their effect on the tropical cyclone structure and intensity is evaluated by artificially modifying the heating and cooling rate due to cloud microphysical processes in the model. The view proposed here is that the effect of diabatic heating in outer spiral rainbands on the storm structure and intensity results mainly from hydrostatic adjustment; that is, heating (cooling) of an atmospheric column decreases (increases) the surface pressure underneath the column. The change in surface pressure due to heating in the outer spiral rainbands is significant on the inward side of the rainbands where the inertial stability is generally high. Outside the rainbands in the far field, where the inertial stability is low and internal atmospheric heating is mostly lost to gravity wave radiation and little is left to warm the atmospheric column and lower the local surface pressure, the change in surface pressure is relatively small. This strong radially dependent response reduces the horizontal pressure gradient across the radius of maximum wind and thus the storm intensity in terms of the maximum low-level tangential wind while increasing the inner-core size of the storm.

The numerical results show that cooling in the outer spiral rainbands maintains both the intensity of a tropical cyclone and the compactness of its inner core, whereas heating in the outer spiral rainbands decreases the intensity but increases the size of a tropical cyclone. Overall, the presence of strong outer spiral rainbands limits the intensity of a tropical cyclone. Because heating or cooling in the outer spiral rainbands depends strongly on the relative humidity in the near-core environment, the results have implications for the formation of the annular hurricane structure, the development of concentric eyewalls, and the size change in tropical cyclones.

1. Introduction

Tropical cyclones (TCs) are rapidly rotating, warm-core atmospheric vortices. A TC typically consists of an eye near its center with little rain, a nearly closed outward-sloping eyewall with strong convection, and both inner and outer spiral rainbands outside the tilted eyewall. Spiral rainbands within a radius of about 2–3 times the radius of maximum wind (RMW) are generally referred to as inner spiral rainbands; those beyond that distance are referred to as outer spiral rainbands. This classification is dynamically consistent, as recently pointed out by Wang (2008a).

Generally, the annular region between the RMW and about 2–3 times the RMW is dominated by the strain flow, in which the strain rate is higher than the relative vorticity (Rozoff et al. 2006). Rozoff et al. (2006) called such an annular region the rapid filamentation zone, where the filamentation time is shorter than the convective overturning time scale. They suggested that all fields in the strain-dominated flow region are rapidly filamented and convection is hypothetically distorted and even suppressed. As a result, Rozoff et al. (2006) proposed that rapid filamentation could play a dynamical role in the formation of the moat—that is, the annular area immediately outside the eyewall, which is an echo-free or a weak echo region as observed on radar

* International Pacific Research Center Publication Number 572 and School of Ocean and Earth Science and Technology Publication Number 7644.

Corresponding author address: Dr. Yuqing Wang, SOEST/IPRC, University of Hawaii at Manoa, 2525 Correa Rd., Honolulu, HI 96822.
E-mail: yuqing@hawaii.edu

DOI: 10.1175/2008JAS2737.1

images of a TC. Based on a full-physics model study, Wang (2008a) demonstrated that instead of suppressing deep convection, the strain-dominated flow region in the rapid filamentation zone outside the RMW provides a favorable environment for well-organized spiral rainbands. Because these rainbands are elongated and sheared, they have characteristics quite different from rainbands outside the rapid filamentation zone. The latter are generally loosely organized in a banded structure with a number of isolated individual convective cells (Wang 2008a). Therefore, the former can be dynamically referred to as inner spiral rainbands, whereas the latter can be referred to as outer spiral rainbands.

An example of the radar reflectivity in a simulated TC in the horizontal and the vertical cross sections is shown in Fig. 1. The simulated TC has a small echo-free eye that is surrounded by a nearly closed eyewall with high reflectivity. Immediately outside the eyewall are the well-organized inner spiral rainbands, which are within a radius of about 60 km or roughly 3 times the RMW. Beyond this region, convection is loosely organized into two major outer spiral rainbands with embedded convective cells.

Recent theoretical and modeling studies have focused mainly on the formation and characteristics of inner spiral rainbands (Montgomery and Kallenbach 1997; Chen and Yau 2001; Wang 2001, 2002a,b; Schecter and Montgomery 2004, 2006, 2007). The predominant view is that the inner spiral rainbands are related to vortex Rossby waves (Montgomery and Kallenbach 1997). These vortex Rossby waves may form as a result of barotropic instability across the elevated potential vorticity (PV) annulus just inside the RMW or as a result of the asymmetric convective activities near the eyewall due to either internal dynamics or environmental forcing (Schubert et al. 1999; Kossin and Schubert 2001; Nolan and Montgomery 2002; Wang 2001, 2002a; Wang and Wu 2004). It is suggested that discrete vortex Rossby waves embedded in the eyewall of a TC are responsible for the formation of the polygonal eyewall structure and eyewall mesovortices, whereas sheared vortex Rossby waves contribute to the formation of inner spiral rainbands (Montgomery and Kallenbach 1997; Kuo et al. 1999; Wang 2001, 2002a,b; Chen and Yau 2001; Nolan and Montgomery 2002; Schecter and Montgomery 2004).

Outer spiral rainbands are predominantly viewed dynamically as inertia–gravity waves (Diercks and Anthes 1976; Kurihara 1976; Willoughby 1978). These waves can be triggered by deep convection in the eyewall, inertial instability in the outflow layer, or variability of the core vorticity distribution (Anthes 1982; Chow et al. 2002; Schecter and Montgomery 2004, 2006). Outer spiral rainbands form quite differently from inner spiral

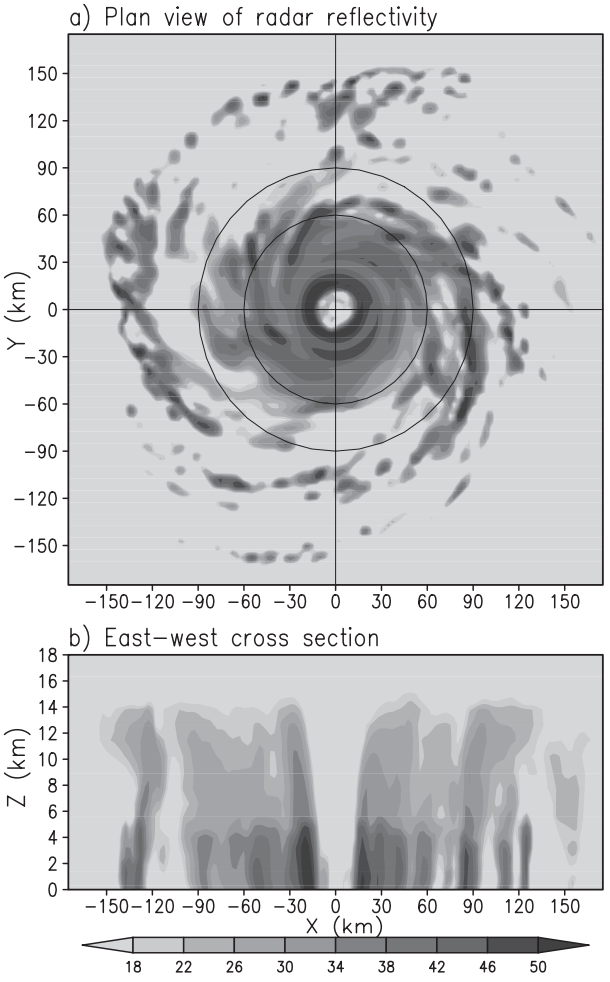

FIG. 1. The model simulated radar reflectivity (in dBZ) after 9 h of simulation in the control experiment after a 48-h spinup for a TC-like vortex on an f plane in a quiescent environment: (a) plan view and (b) vertical cross section along the east–west direction across the storm center. Two circles in (a) show the radii of 60 and 90 km from the storm center, respectively.

rainbands. Wang (2001, 2002a,b) showed in his TC model that outer spiral rainbands most frequently form and develop between 80 and 150 km from the TC center. This preferred region, according to Willoughby et al. (1984), results from the effect of downdrafts from clouds in the outflow layer. That is, outer spiral rainbands are determined by the outflow radial wind speed and the terminal velocity of the ice species (snow, graupel) in the upper part of the eyewall, which may lead to a radius of about 100 km in strong TCs. This explanation is supported by Wang (2002c), who showed in his full-physics model simulations that when the melting of snow and graupel and the evaporation of rain are turned off, the outer spiral rainbands are largely suppressed or even disappear.

Regardless of the formation mechanisms of outer spiral rainbands, the objective of this study is to understand how they affect the overall structure and intensity of a TC. Previous studies (Barnes et al. 1983; Powell 1990a,b; Wang 2002b,c) suggest that spiral rainbands may affect TC intensity markedly through several different physical processes. Dynamically, the mass convergence into spiral rainbands may reduce the mass convergence into the eyewall, which will decrease the eyewall updrafts and convection and weaken the TC. Alternatively, the compensating subsidence resulting from the convective overturning in spiral rainbands may introduce dry air that could suppress eyewall convection and limit TC intensity (Willoughby et al. 1982; Shapiro and Willoughby 1982). Wang (2002b) showed in his model that perturbations to the eyewall by outer spiral rainbands can lead to a breakdown of the eyewall and thus weaken the TC. Blocking of the boundary layer inflow is found to be a critical factor in such an eyewall breakdown and associated intensity decrease.

Strong downdrafts associated with convective activity and anvil clouds in outer spiral rainbands can exert a thermodynamic effect on TC structure and intensity. Downdrafts can bring low equivalent potential temperature (θ_e) air from the middle troposphere down to the inflow boundary layer. Unless these low values of θ_e are restored by extracting heat and moisture from the ocean surface as the air spirals inward in the boundary layer, the eyewall buoyancy/convection and thus the TC intensity will be reduced (Barnes et al. 1983; Powell 1990a,b). Another thermodynamic effect that will be discussed in this study is the hydrostatic adjustment associated with the net diabatic heating in outer spiral rainbands and anvil clouds. Such heating outside the eyewall may cause pressure to fall in the lower troposphere and reduce the pressure gradient across the eyewall, which will weaken the tangential wind near the RMW but increase the size of the TC inner core.

Whereas the above arguments all suggest that the outer spiral rainbands limit TC intensity, May and Holland (1999) suggested that cyclonic PV anomalies could be generated in the midtroposphere stratiform cloud region associated with spiral rainbands. They hypothesized that the transfer of this cyclonic PV to the TC core region could be a considerable PV source to the TC core. As a result, spiral rainbands might act to increase TC intensity. In an idealized full-physics model simulation, Wang (2008b) found that interaction between the eyewall and inner spiral rainbands can lead to a size increase of the storm's eye and eyewall and the formation of an annular hurricane.

The objective of this study is to understand, on the basis of idealized numerical experiments with a nonhydrostatic, cloud-resolving TC model, how outer spiral rainbands affect the TC structure and intensity. The particular focus is on the hydrostatic adjustment mechanism associated with diabatic heating in outer spiral rainbands and anvil clouds outside the inner core. The rest of the paper is organized as follows: Sections 2 and 3 describe the numerical model and the experimental design, respectively. Section 4 discusses the model results, with a focus on the effect of the outer spiral rainbands on both the intensity and structure changes of the model TC. Implications of the model results are discussed in section 5. The main conclusions are drawn in the last section.

2. The tropical cyclone model TCM4

The model used in this study is the fully compressible, nonhydrostatic, primitive equation model TCM4 recently developed by the author at the International Pacific Research Center, University of Hawaii. TCM4 is an upgrade of its counterpart TCM3 (Wang 2001, 2002c), with the hydrostatic dynamical core replaced by a fully compressible, nonhydrostatic dynamical core. Wang (2007) used TCM4 to analyze the development of asymmetries in the inner core and the inner-core structure and intensity changes in a TC at nearly cloud-resolving resolutions. Wang (2008a,b) recently applied the model to examine the rapid filamentation zone in TCs as conceptualized by Rozoff et al. (2006) and to investigate the three-dimensional structure and formation mechanism of annular hurricanes identified in observations by Knaff et al. (2003). Because a full description of TCM4 can be found in Wang (2007), only the major features of the model are described below.

The TCM4 model has the same state-of-the-art model physics, two-way interactive multiple nesting, and automatic mesh movement as its hydrostatic counterpart TCM3 (Wang 2001, 2002c). The model equations are formulated in Cartesian coordinates in the horizontal and mass coordinates in the vertical and are solved numerically with an efficient forward-in-time, explicit time-splitting scheme that is similar to the scheme of Wicker and Skamarock (2002). A fifth-order (second-order) upwind scheme, which takes into account the effect of spatial variation of the advective flow (Wang 1996), is used to calculate the time tendency due to horizontal (vertical) advection. The model lower boundary is a flat surface with an unperturbed surface pressure of 1010 hPa. The model top is set at about 38 km and has a sponge upper boundary condition similar to that in Durran and Klemp (1983) to absorb the upward-propagating sound and gravity waves. The model physics include an E–ε turbulence closure scheme for subgrid-scale vertical turbulent mixing (Langland and Liou 1996), a modified

Monin–Obukhov scheme for surface flux calculations (Fairall et al. 2003), an explicit treatment of mixed-phase cloud microphysics (Wang 2001), a nonlinear fourth-order horizontal diffusion for all prognostic variables except for those related to the mass conservation equation, a simple Newtonian cooling term [which is added to the perturbation potential temperature equation to mimic the radiative cooling in the model (Rotunno and Emanuel 1987)], and dissipative heating due to molecular friction related to the turbulent kinetic energy dissipation rate ε from the E–ε turbulent closure scheme.

The model domain is quadruply nested with two-way interactive nesting and with inner meshes that automatically move to follow the model storm, as in TCM3 (Wang 2001). The model has 26 levels in the vertical with relatively high resolution both in the lower troposphere and near the tropopause. The model simulations in this study are not sensitive to the number of vertical levels (Zhang and Wang 2003; Kimball and Dougherty 2006). The horizontal grid intervals of 67.5, 22.5, 7.5, and 2.5 km have domain sizes of 251 × 151, 109 × 109, 127 × 127, and 163 × 163 grid points for the four meshes, respectively.

As in Wang (2007, 2008a,b), the same model physics are used in all meshes. Because no large-scale environmental flow is included in this study, convection is mainly active in the inner-core region and in the spiral rainbands that are within a radius of about 200 km from the cyclone center and thus are within the finest innermost domain. Therefore, cumulus parameterization is not considered even in the two outermost meshes in this study.

3. Experimental design

The experimental design follows Wang (2008a,b). The model is initialized with an axisymmetric cyclonic vortex on an f plane of 18°N in a quiescent environment over the ocean with a constant sea surface temperature of 29°C. The initial thermodynamic structure of the unperturbed model atmosphere is defined as the western Pacific clear-sky environment given by Gray et al. (1975). The initial cyclonic vortex has a maximum tangential wind speed at the surface of 20 m s^{-1} at a radius of 80 km, which then decreases sinusoidally with pressure and vanishes at 100 hPa. The mass and thermodynamic fields are obtained by solving the nonlinear balance equation as described in the appendix of Wang (2001).

After a spinup period of 48 h with all default model parameters, the model TC develops a structure similar to real TCs (Fig. 2) in terms of tangential and radial winds, vertical velocity, temperature anomalies, PV, and relative angular momentum. The maximum tangential wind near the surface occurs at a radius of about 18 km (Fig. 2a). The storm developed a shallow inflow in the boundary layer and an outflow layer in the upper troposphere (Fig. 2b). The eyewall ascent slopes radially outward with height, especially in the middle and upper troposphere (Fig. 2c). The storm has a warm core structure in the middle and upper troposphere, with a maximum temperature anomaly greater than 9 K at the given time (Fig. 2d). The PV has an off-center maximum just within the RMW throughout the troposphere (Fig. 2e). The angular momentum surface in the radial–height plane is quite erect in the eye region but increasingly tilts outward with height outside of the eyewall (Fig. 2f). The eyewall ascent (Fig. 2c) follows the angular momentum surface and coincides with both the largest radial gradient of angular momentum (Fig. 2f) and the outer edge of the elevated PV annulus in the mid-to-lower troposphere (Fig. 2e). These features are consistent with both observations and previous model results.

Because outer spiral rainbands are mainly driven by diabatic heating due to phase changes in the rainbands, their effect on TC intensity and structure can be evaluated by artificially modifying the heating and cooling rates calculated from the cloud microphysics in the model. In the cloud-resolving model TCM4, the heating rate due to phase changes in cloud microphysics includes heating due to condensation, deposition, and freezing, while the cooling rate includes cooling due to sublimation of ice particles, evaporation of rain and cloud droplets, melting of snow and graupel, and evaporation of melting snow and graupel (Wang 2001). To investigate the effects of heating and cooling separately, the total diabatic heating rate Q calculated from cloud microphysics at a given time step at a grid point is decomposed into the net heating rate Q^+ and the net cooling rate Q^-; that is,

$$Q = Q^+ + Q^- = \max(Q,\ 0.0) + \min(Q,\ 0.0). \quad (1)$$

Note that for a given grid point in three dimensions at a time step, Q equals either Q^+ or Q^-. To focus on the effect of net heating/cooling in the outer spiral rainbands on the TC structure and intensity, two parameters α and β are introduced to modify the net heating rate Q^+ and the net cooling rate Q^-, respectively:

$$Q^* = \alpha Q^+ + \beta Q^-. \quad (2)$$

Two functions F_1 and F_2 are introduced as follows:

$$F_1 = \begin{cases} 100\%, & \text{for } r \le 60 \text{ km}; \\ 100\% - 20\%(r - 60)/30, & \text{for } 60 \text{ km} < r < 90 \text{ km}; \\ 80\%, & \text{for } r \ge 90 \text{ km}; \quad \text{and} \end{cases} \quad (3)$$

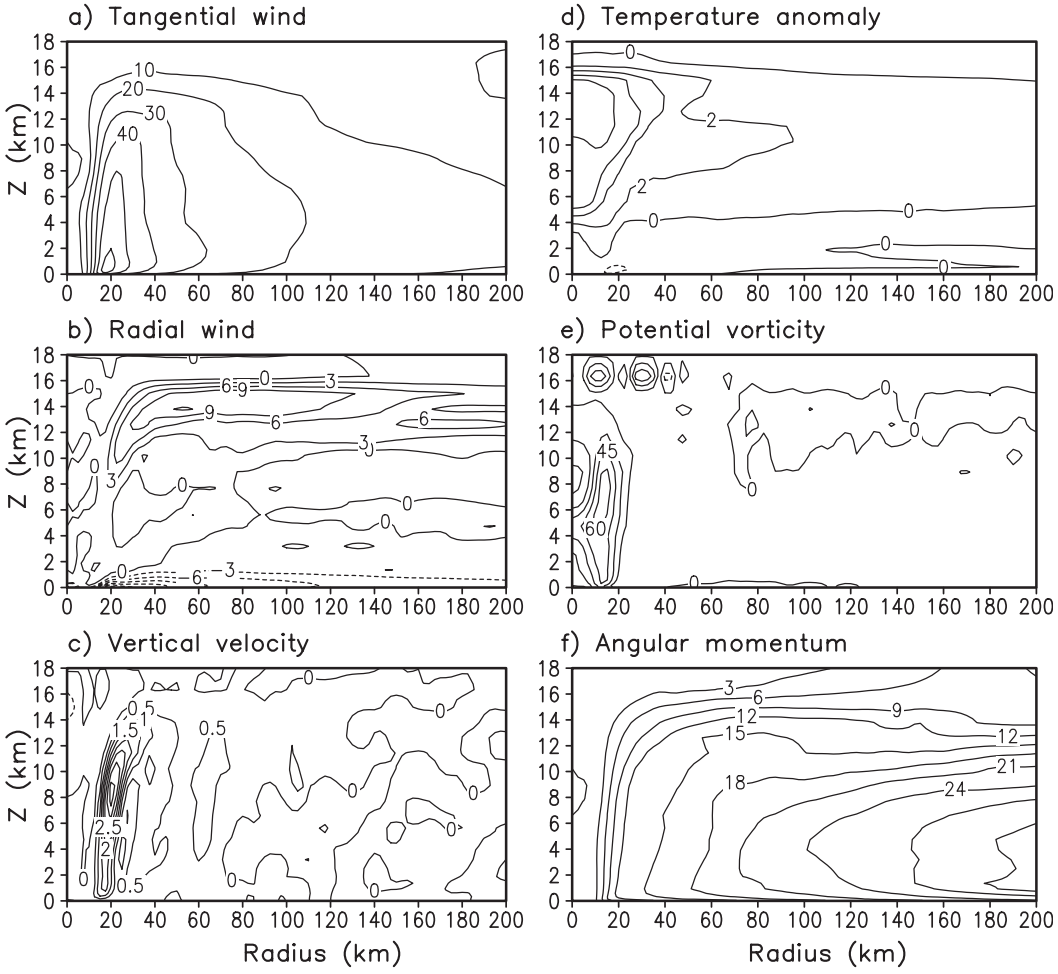

FIG. 2. The azimuthal mean structure of the model tropical cyclone after the 48-h spinup: (a) tangential wind [contour interval (CI) = 10 m s^{-1}], (b) radial wind (CI = 3 m s^{-1}), (c) vertical velocity (CI = 0.5 m s^{-1}), (d) perturbation temperature (CI = 2 K), (e) potential vorticity (CI = 5 PVU), and (f) relative angular momentum (CI = 3×10^5 m^2 s^{-1}).

$$F_2 = \begin{cases} 100\%, & \text{for } r \le 60 \text{ km}; \\ 100\% + B(r - 60)/30, & \text{for } 60 \text{ km} < r < 90 \text{ km}; \\ 100\% + B, & \text{for } r \ge 90 \text{ km}; \end{cases} \quad (4)$$

where r is the radial distance from the model TC center in kilometers and B is a fraction of percentage, which will be specified in different experiments below. The radii of 60 and 90 km were chosen based on the fact that outer spiral rainbands are active outside these radii with the standard model settings (Fig. 1). The cutoff at a radius of 60 km was chosen so as not to affect the heating/cooling rate of the eyewall or of the inner spiral rainbands and to modify the activity of only the outer spiral rainbands outside the inner core.

Six numerical experiments (Table 1) were conducted in which the net heating/cooling rate calculated from the cloud microphysics module was varied. In these experiments, the calculated net heating/cooling rate Q from cloud microphysics was replaced by the modified net heating/cooling rate Q^* at each time step and a given grid point according to (2) in the model. In the control experiment (CTRL), $\alpha = \beta = 1$; that is, all model settings are the same as those used in the model spinup (namely, the standard settings). In experiment HC80, $\alpha = \beta = F_1$; that is, the net heating and cooling rates due to phase changes in cloud microphysics are linearly reduced from 100% at a radius of 60 km to 80% of that calculated at a radius of 90 km, and the rates remain 80% outward. In experiment C80 (H80), the net cooling (heating) rate is reduced linearly from 100% calculated at a radius of 60 km to 80% of that calculated at a radius of 90 km and remains 80% outward; that is, $\alpha = 1$ and $\beta = F_1$ in C80, and $\alpha = F_1$ and $\beta = 1$ in H80.

TABLE 1. Summary of the numerical experiments performed in this study.

Experiment	Comments on the experimental design
CTRL	Standard model settings [$\alpha = \beta = 1$ in (2)]
HC80	Both heating and cooling rates due to phase change in cloud microphysics are reduced to 80% outside 90 km from the storm center (i.e., $\alpha = \beta = F_1$)
C80	Cooling rate due to phase change in cloud microphysics is reduced to 80% outside 90 km from the storm center (i.e., $\alpha = 1, \beta = F_1$)
H80	Heating rate due to phase change in cloud microphysics is reduced to 80% outside 90 km from the storm center (i.e., $\alpha = F_1, \beta = 1$)
C120	Cooling rate due to phase change in cloud microphysics is increased by 20% outside 90 km from the storm center [i.e., $\alpha = 1, \beta = F_2$ with $B = 20\%$ in (4)]
H110	Heating rate due to phase change in cloud microphysics is increased by 10% outside 90 km from the storm center [i.e., $\alpha = F_2$ with $B = 10\%$ in (4) and $\beta = 1$]

In experiment C120, the net cooling due to phase changes in cloud microphysics is increased linearly from 100% at a radius of 60 km to 120%; similarly, in H110 the net heating rate increases to 110% of that calculated at a radius of 90 km. The rates remain 120% and 110% outward, respectively; that is, $\alpha = 1$ and $\beta = F_2$ with $B = 20\%$ in C120, and $\alpha = F_2$ with $B = 10\%$ and $\beta = 1$ in H110. These experiments are primarily designed to understand how important the diabatic heating (or cooling or both) due to phase changes in the outer spiral rainbands is to the model TC structure and intensity. Strictly speaking, increasing or reducing the heating/cooling rate according to (2) and (3) includes heating/cooling in the stratiform anvil clouds in the middle and upper troposphere outside the inner core. Nevertheless, for convenience in the following discussion, no distinction will be made between heating/cooling in outer spiral rainbands and that in anvil clouds outside the inner core.

The modifications to the heating rate require an accurate determination of the storm center, which is defined as the circulation center with the maximum axisymmetric tangential wind. The azimuthal mean modified heating rates Q^* in the six experiments after 9 h of integration are shown in Fig. 3. Note that cooling occurs mainly in the middle and lower troposphere, but heating can occur in deep convective clouds and also in stratiform clouds in the middle and upper troposphere (Figs. 1b and 3a). Because the surface pressure response to diabatic heating/cooling is much larger in the upper troposphere than in the lower troposphere (e.g., Holland 1997), the heating rate was increased by only 10% outside the inner core in H110 to avoid a too-quick expansion of the model TC.

4. Results

The evolution of the maximum azimuthal-mean tangential wind at the lowest model level (about 35 m above the sea surface) and the minimum surface pressure at the storm center for all six experiments are shown in Fig. 4. The storm in the control experiment intensified the first day and then evolved steadily, slowly increasing in intensity until day 4 and then slightly weakening after day 6. Reducing both the heating and cooling rates outside the inner core in the HC80 experiment results in a TC that intensifies rapidly for the first 3 days and then continues to gradually intensify until it reaches a maximum azimuthal mean tangential wind speed of about 77 m s^{-1} and a minimum central surface pressure of 887 hPa, the lowest surface pressure among the six experiments.

This greater intensification in HC80 than in CTRL was mainly due to the reduced heating rate rather than the reduced cooling rate, because the storm in experiment H80 intensified more rapidly and in C80 more slowly than in CTRL. This implies that cooling in the outer spiral rainbands is not prohibitive to, but promotes TC intensity; whereas heating in the outer spiral rainbands inhibits TC intensification and intensity. The results from experiments C120 and H110 support this point. Similarly, a higher cooling rate in the outer spiral rainbands in C120 results in a more rapid intensification and greater intensity of the storm than in CTRL, whereas a higher heating rate in H110 results in more gradual intensification (even weakening) and a less intense storm than in CTRL (Fig. 4). Although the storm in H110 weakened for about 3 days (Fig. 4a), its subsequent intensification is attributable to the increase of its inner-core size with time because the radial profile in (4) was time-independent, and the increased heating rate occurred within the eyewall of the storm at a later stage. The storm in H110 also experienced interesting eyewall cycles, which will be discussed later.

Because cooling due to evaporation of rain, melting of snow and graupel, and evaporation of melting snow and graupel is the major contributor to downdrafts in outer spiral rainbands (Franklin et al. 2005), the above

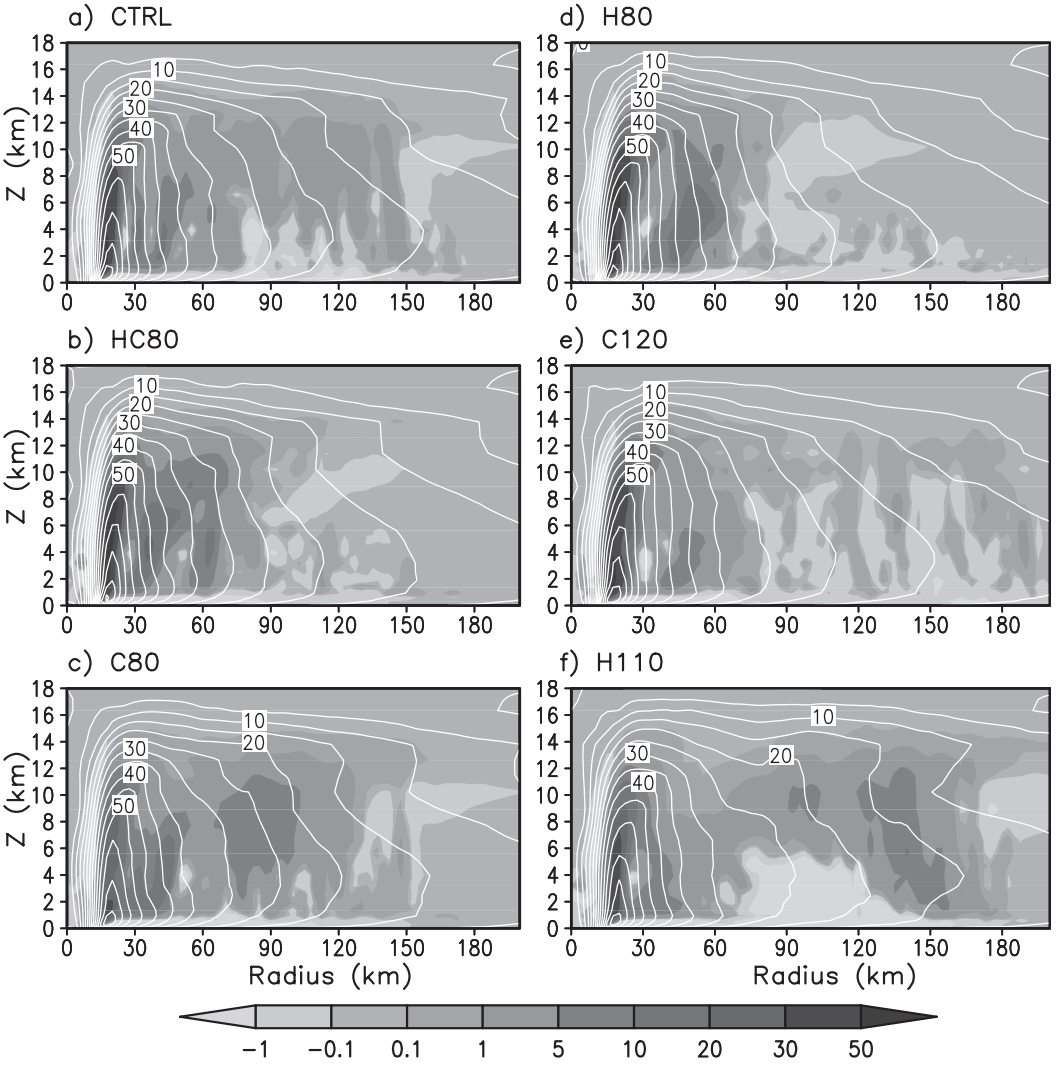

FIG. 3. Radial–vertical distributions of the azimuthal mean net diabatic heating rate due to phase changes from the model cloud microphysics scheme (K h^{-1}; shading) and tangential wind (m s^{-1}) after 9 h of integration in experiments (a) CTRL, (b) HC80, (c) C80, (d) H80, (e) C120, and (f) H110.

results imply that downdrafts in outer spiral rainbands can intensify a TC. Bister (2001) found that suppression of convection outside the core by artificially reducing the surface sensible and latent heat fluxes in the outer region of the model vortex resulted in earlier onset of rapid intensification. However, Bister did not examine whether it was heating or cooling in the outer region that contributed to the earlier intensification. In these simulations (Fig. 4), it is clear that it is cooling that leads the more rapid intensification and the stronger storm.

A distinct feature is the difference in size of the eye and eyewall in the simulated storm, as seen from the surface rain rate after 120 h of integration in Fig. 5. Reducing the heating rate in H80 or increasing the cooling rate in C120 in the outer spiral rainbands considerably reduced the size of the eye and eyewall (Figs. 5d,e) compared to the control experiment (Fig. 5a). Reducing both the heating and cooling rates in HC80 (Fig. 5b) leads to a slightly wider eyewall than in CTRL but a similar inner-core size (Fig. 5a). In contrast, reducing the cooling rate in C80 and increasing the heating rate in H110 in the outer spiral rainbands results in a tremendous increase in eye and eyewall size (Figs. 5c,f). Note that the rain rate in the C80 eyewall is much higher than in H110, a result consistent with the much weaker H110 storm (Fig. 4).

Another important feature in Fig. 5 is the difference in the rain structure outside the inner core in the simulated storms. In CTRL, some outer spiral rainbands occur beyond a radius of 90 km (Figs. 1 and 5a). No major

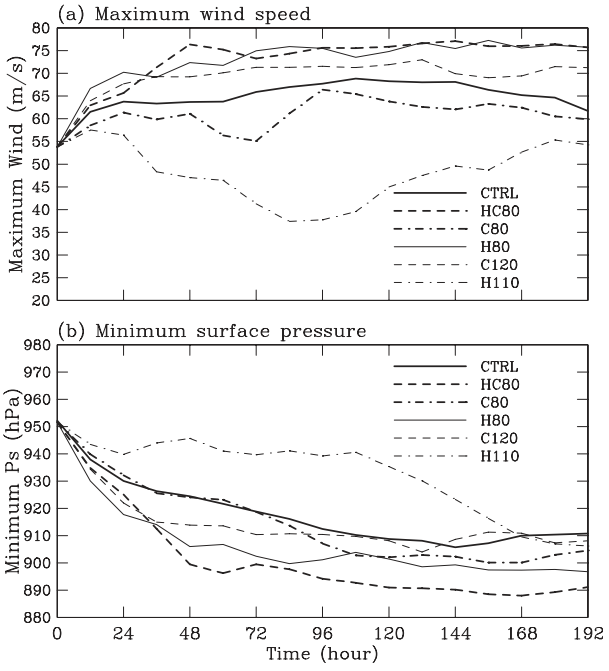

FIG. 4. Time evolution of (a) the maximum azimuthal mean wind speed (m s^{-1}) at the lowest model level (35.6 m above the sea surface) and (b) the minimum central surface pressure (hPa) in all six experiments as given in Table 1.

outer spiral rainbands developed with the reduced heating and cooling rates in HC80, the reduced heating rate in H80, or the increased cooling rate in C120 (Figs. 5b,d,e). The absence of active outer spiral rainbands under these conditions indicates that heating is critical to the maintenance of outer spiral rainbands, whereas cooling is destructive. The stronger storms in HC80, H80, and C120 than in CTRL imply that outer spiral rainbands weaken a storm. Although outer spiral rainbands developed in the early stage of C80, they were greatly suppressed in the later stage, mainly because of the development of the annular hurricane structure (see later discussion). However, the active outer spiral rainbands in H110 contributed to the fact that this was the weakest of the six storms in terms of the maximum low-level azimuthal mean tangential wind (Fig. 4). In addition to the snapshot of rain rate shown in Fig. 5, the difference in the outer rainbands is evident in the radial distribution of the azimuthal-mean rain rate averaged between 72 and 144 h of simulation (Fig. 6). The relatively high rain rate beyond the 60–90-km radius in CTRL compared to HC80, H80, and C120 is a manifestation of the existence of active outer spiral rainbands in CTRL.

Large differences in the vertical structure of the azimuthal-mean vertical motion and of tangential wind exist among the six simulated storms (Fig. 7). The eyewalls of the small-eye storms in experiments CTRL, HC80, H80, and C120 are nearly vertical in the lower and middle troposphere and then start to tilt outward (Figs. 7a,b,d,e). However, in the large-eye C80 and H110 storms, the eyewall slopes outward quite steeply (Figs. 7c,f). Wang (2008b) demonstrated that the large outward eyewall tilt is a necessary condition for the maintenance of large-eye storms because the response of the low-level tangential wind to heating in the outwardly titled eyewall is an increase outside and a decrease near and inside the RMW, preventing an inward contraction or even inducing an expansion of the RMW (Shapiro and Willoughby 1982; Wang 2008b).

The RMW in the CTRL experiment increased by 2.5 km between days 2 and 3 and then increased again by 5 km after 7 days of simulation (Fig. 8). The last increase in the RMW in CTRL is the result of the development of an annular hurricane (Wang 2008b), a storm with a wide eyewall and weak outer spiral rainbands, as documented from observations by Knaff et al. (2003). The RMW in HC80 remained small and increased only by 2.5 km after 3 days of simulation and did not become an annular hurricane throughout the 8-day simulation. The RMW in H80 decreased by 2.5 km after 1 day of simulation and then remained at 12.5 km afterward. With the cooling rate increased by 20% outside the inner core in C120, the storm had a comparatively small RMW that decreased to 10 km after 6 days of simulation. Results from both H80 and C120 indicate that cooling in the outer spiral rainbands contributes positively to the intensity and favors a small eye and eyewall in a TC.

Dramatic changes in the RMW occurred in experiments C80 and H110 (Fig. 8). In C80, the RMW of the storm increased continuously with time with a notable rapid increase between 60 and 78 h of simulation. The rapid increase in the RMW is a result of the transition from a regular hurricane structure to an annular hurricane structure, similar to that described in Wang (2008b) with the same TC model (TCM4). In H110, the RMW remained small for the first 3 days and then increased significantly with two jumps: one from 17.5 to 70 km during 84 and 90 h and the other from 80 to 110 km during 144 and 160 h of simulation, respectively. These abrupt RMW increases are closely related to the formation and replacement of the concentric eyewall structure as described by Willoughby et al. (1982). The only difference here is the lack of contraction of the new eyewall due to the increased heating rate outside the original RMW by design (see section 2).

Although the formation of the annular hurricane in C80 is quite similar to that described in Wang (2008b), the transition from the regular hurricane to the annular

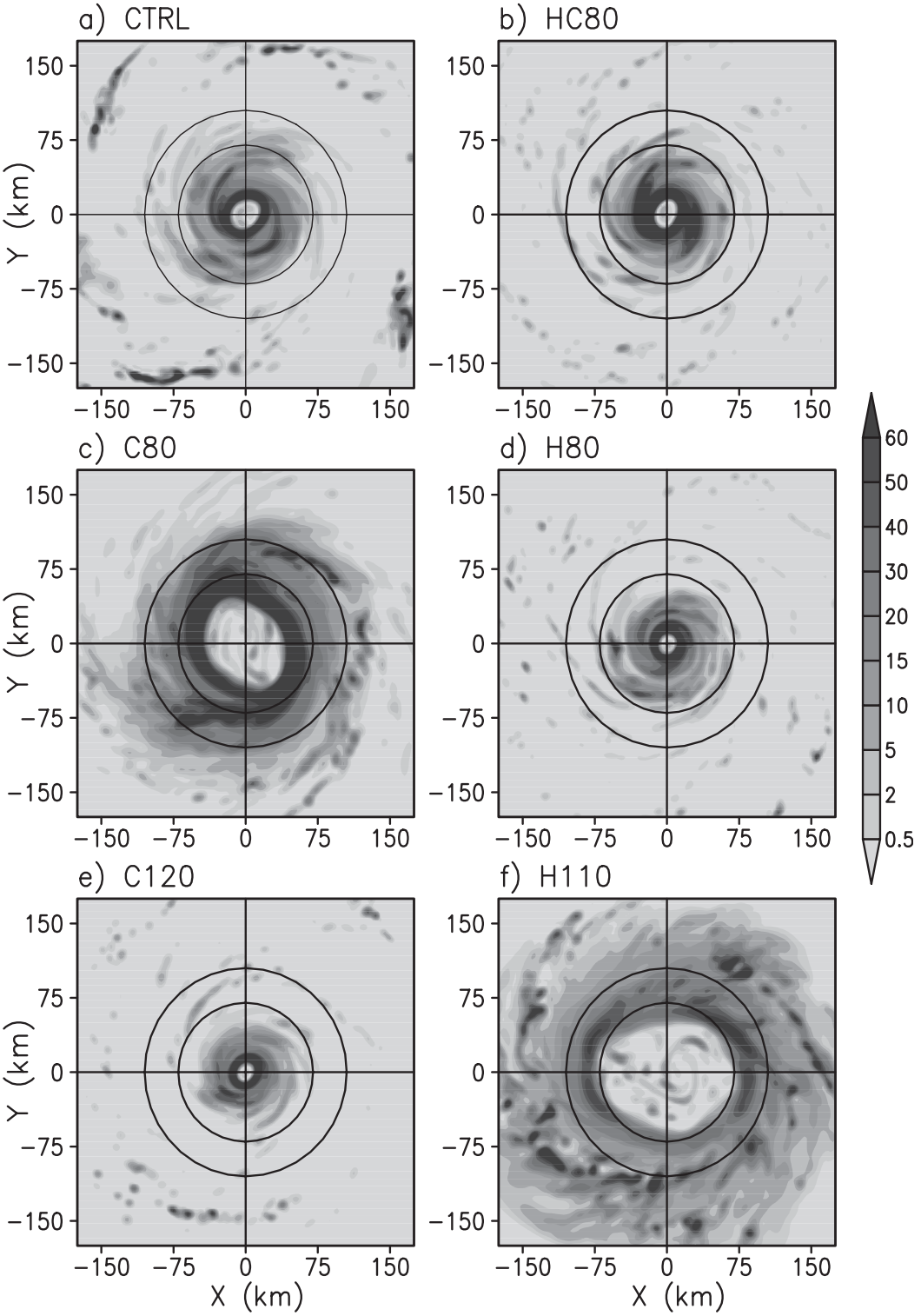

FIG. 5. The plan view of the rain rate (mm h^{-1}) of the model tropical cyclones after 120 h of simulation from experiments (a) CTRL, (b) HC80, (c) C80, (d) H80, (e) C120, and (f) H110. Two circles in each panel show the radii of 60 and 90 km from the storm center, respectively.

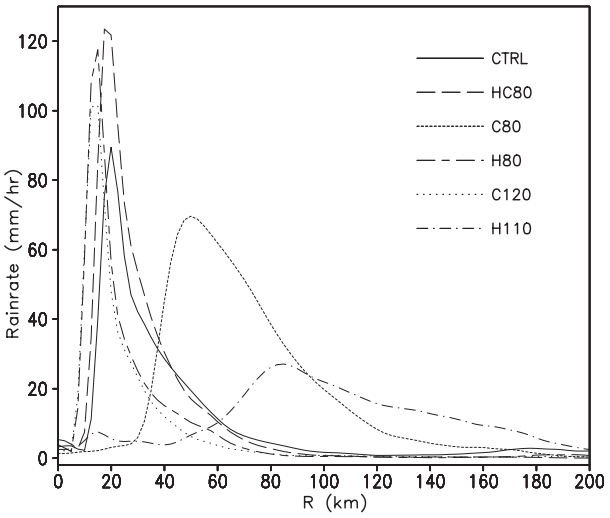

FIG. 6. Radial distribution of the azimuthal mean rain rate averaged between 72 and 144 h of simulations from the six experiments as given in Table 1.

hurricane in C80 occurred between 30 and 72 h of simulation (Fig. 9) and much earlier than that in Wang (2008b). This suggests that the reduced cooling rate outside the inner core favors formation of annular hurricanes. The formation of the annular hurricane in C80 also resulted from several eyewall cycles associated with the interaction between the eyewall and inner spiral rainbands, similar to those discussed in Wang (2008b). The first eyewall cycle occurred between 30 and 42 h of simulation. Inner spiral rainbands that developed after 30 h of simulation were axisymmetrized to form a quasi-symmetric convective ring that propagated inward and impinged on and merged with the eyewall convection by 39 h (Figs. 9 and 10). The second and third similar eyewall cycles occurred between 42 and 60 h and between 60 and 78 h of simulation, after which an annular-type storm formed with wide eyewall and weak outer spiral rainbands. As indicated in Wang (2008b), the convective ring that formed outside the eyewall was generally too close to the RMW to have a separate local tangential wind maximum, which is quite different from the concentric eyewall cycle described by Willoughby et al. (1982). As discussed in Wang (2008b), the large outward tilt of the eyewall (Fig. 7c) is critical to the maintenance of the large-eye annular hurricane.

Although no concentric eyewall cycle was simulated in CTRL, the storm in H110 developed a typical concentric eyewall structure and associated eyewall replacement (Fig. 11). The first concentric, secondary eyewall formed after about 27 h of simulation as a result of the axisymmetrization of the inward-propagating spiral rainbands. As the secondary eyewall formed and contracted, the inner eyewall started to weaken and eventually was replaced by the secondary eyewall at about 45 h of simulation. In contrast to the typical concentric eyewall cycle described by Willoughby et al. (1982), no secondary azimuthal-mean tangential wind maximum was associated with the secondary convective ring (Fig. 12). As with the formation of the annular hurricane structure in C80, the secondary convective ring formed in the first episode was too close to the RMW to develop its own local tangential wind maximum. The second episode occurred during 51 and 78 h of simulation (Figs. 11 and 12) and had many characteristics of the typical concentric eyewall cycle of Willoughby et al. (1982), such as the formation and subsequent contraction of the secondary, outer eyewall with its own local tangential wind maximum and the weakening of the primary, inner eyewall. However, the eyewall replacement was not completed in the simulation because the inner eyewall also contracted and was maintained for a very long time (Figs. 11 and 12). The third episode during 81 and 108 h of simulation had a typical concentric eyewall structure with a relatively wide moat between the primary and secondary eyewalls. The formation of the secondary eyewall in the third episode seemed to result from the axisymmetrization of outer spiral rainbands. This third secondary eyewall slightly expanded after its formation (Figs. 11 and 12). The inner eyewall eventually broke down and dissipated after 111 h of simulation, leaving a very large eye structure.

The expansion and intensification of the single large eyewall after 108 h of simulation in H110 can be attributed to the increased heating rate outside the 60–90-km radius because the new eyewall is outside this radius (Fig. 8). Another mechanism for the expansion of the secondary eyewall in the third episode is its large outward tilt (Fig. 13), which prevents the eyewall from contracting, as explained by Shapiro and Willoughby (1982). That is, heating outside the RMW in the mid-troposphere, such as heating in the outwardly tilted eyewall, will increase (reduce) low-level tangential wind outside (near and inside) the RMW and lead to the outward expansion of the RMW or prevent the inward contraction of the RMW.

Both the intensity and structure changes discussed above can be understood in terms of hydrostatic adjustment. Internal atmospheric diabatic heating (cooling) is expected to warm (cool) the atmospheric column and thus reduces (increases) the surface pressure. Therefore, reducing the heating rate in H80 or increasing the cooling rate in C120 outside the inner core would increase the surface pressure outside the RMW and increase the pressure gradient across the RMW (Figs. 14d,e) and thus increase the maximum tangential wind and the storm

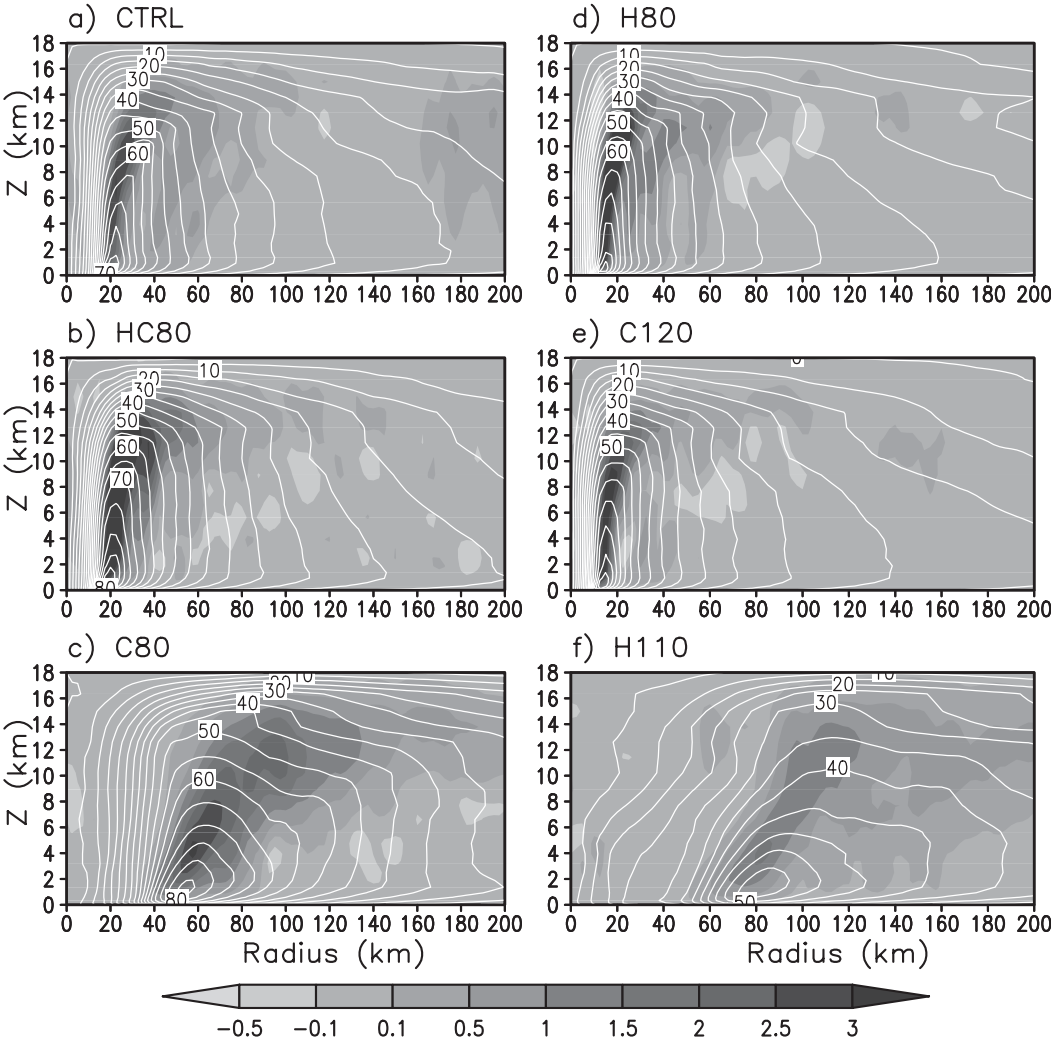

FIG. 7. Radial–vertical structure of the azimuthal mean vertical motion (m s^{-1}; shading) and tangential wind (contours; CI = 5 m s^{-1}) in the model tropical cyclones after 120 h of simulation from experiments (a) CTRL, (b) HC80, (c) C80, (d) H80, (e) C120, and (f) H110.

intensity (Fig. 4a). Increasing the pressure gradient outside the RMW prevents growth of the storm inner core, which leads to the smallest storms in the two experiments (Figs. 5d,e). By contrast, reducing the cooling rate outside the inner core in C80 lowers the surface pressure outside the RMW (Fig. 14c) and thus reduces the pressure gradient across the RMW but increases it outside the RMW. Both effects weaken the storm but increase the size of the inner core compared to that in CTRL (Figs. 14a,c).

Although increasing the heating rate outside the inner core by 10% in H110 is also expected to lower the surface pressure outside the RMW, this did not lead to an immediate increase of the RMW (Fig. 8). Instead, the storm only intensified at a slower rate in the first day than in the CTRL and then weakened considerably until day 4 (Fig. 4). This dramatic decrease in intensity is attributable to the development of the secondary eyewall, as already discussed above. A rapid increase in the eye and eyewall diameter between 108 and 168 h of simulation is evidently due to the fact that part of the eyewall was within the increased heating rate region (outside 60 km). As a result, the inner core expanded with a slow intensification after about a 4-day simulation in H110 (Figs. 4 and 8).

The correlation between the surface pressure drop and the surface rain rate outside the inner core (Fig. 14) supports the above hydrostatic adjustment argument. The surface rain rate reflects the net internal atmospheric diabatic heating due to phase changes in model cloud microphysics. The lack of significant surface rainfall outside a radius of 80–90 km in HC80, H80, and C120

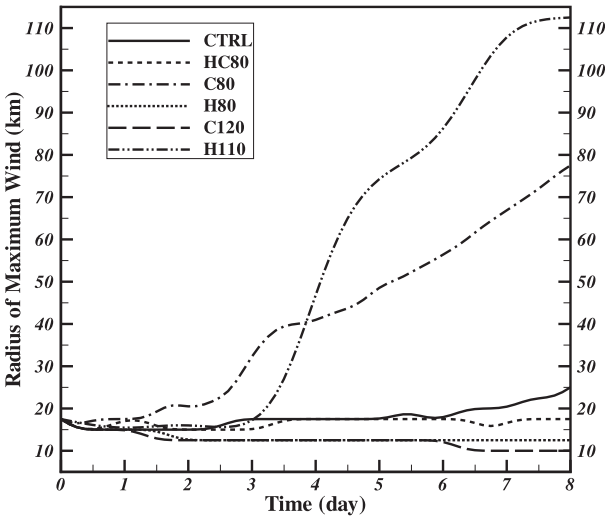

FIG. 8. Time evolution of the radius of maximum wind (km) in all six experiments.

(Figs. 14b,d,e) implies little internal atmospheric heating outside the inner core. This is in contrast to the considerable rainfall and internal atmospheric heating, which give rise to the lower surface pressure outside the inner core in CTRL, C80, and H110 (Figs. 14a,c,f) and an increase in the inner-core size of the storms in these experiments (Fig. 8). The hydrostatic adjustment mechanism can be easily seen in the radial distribution of the column-integrated net heating rate and the perturbation sea level pressure averaged between 72 and 144 h of simulation (Figs. 15a,b). The pressure decrease is highly correlated with the net internal atmospheric heating rate. Heating in the outer spiral rainbands changes surface pressure significantly on the inward side of the rainbands in the inner-core environment but changes it relatively little outside the rainbands in the far field (Fig. 15; see also Shapiro and Willoughby 1982). The significant effect on surface pressure in the inner-core region is mainly due to the fact that the inertial stability is high in the inner- and near-core environment (Fig. 16), where internal atmospheric heating can effectively warm the atmospheric column and lower the surface pressure (Hack and Schubert 1982). Outside the rainbands, however, inertial stability is low and internal atmospheric heating is mostly lost to gravity wave radiation, leaving little to warm the atmospheric column and to lower the local surface pressure.

In addition to the hydrostatic adjustment, increasing or reducing the heating or cooling rate may modify the vertical structure of the atmosphere and thus convection (Fig. 17). Consistent with the artificially modified heating/cooling rates, the temperature anomalies averaged between 72 and 96 h of integration are much smaller outside the radius of 60–90 km in HC80, H80, and C120 than in CTRL, which may be due to either the reduced heating or increased cooling rate or the lack of active outer spiral rainbands (Fig. 5). In C80 and H110, the temperature anomalies (warm core) extend to much larger radii than in CTRL, which is consistent with the large eye and eyewall and the smaller intensity during this period (Figs. 4 and 8). This extension of the warm core in the upper troposphere provides a more stable vertical structure in the near-core environment, which favors the outward tilt of the eyewall ascent and thus large eyewall slope (Fig. 6). Whereas Persing and Montgomery (2005) stated that the maximum intensity of their model TCs was not sensitive to the initial environmental convective available potential energy (CAPE), the TC intensity during this period in these simulations appears to be closely related to CAPE, as can be inferred from the vertical profile of the equivalent potential temperature in the near-core environment (Figs. 4 and 17). For example, the HC80 experiment has the most conditionally unstable condition for convection (Fig. 17b) and gives the most intense storm.

The above discussions have been based on the axisymmetric dynamics. Diabatic heating/cooling in outer spiral rainbands generally has both symmetric and asymmetric components (Fig. 1; also see Wang 2008a). In addition to the symmetric component, the asymmetric component of diabatic heating in outer spiral rainbands might play some role in modifying the overall storm structure and intensity as well. However, Nolan and Grasso (2003) found that although asymmetric temperature perturbations due to diabatic heating have a negative effect on overall intensity of a three-dimensional balanced TC vortex, the resultant change is about two orders of magnitude smaller than those caused by symmetric perturbations of equal amplitude. Therefore, it is unlikely that the asymmetric component of diabatic heating in outer spiral rainbands contributes significantly to the overall storm intensity and structure in these simulations.

5. Discussion

Previous views on the effects of outer spiral rainbands on TC intensity have been mainly based on three arguments: blocking of the boundary layer inflow, subsidence forced by diabatic heating in outer spiral rainbands, and the cooling and drying of the boundary layer inflow due to convective downdrafts. The first two effects are dynamical effects; the last is a thermodynamic effect. Another less frequently discussed effect, proposed by May and Holland (1999), is the inward transport of potential vorticity generated in outer spiral rainbands, which could

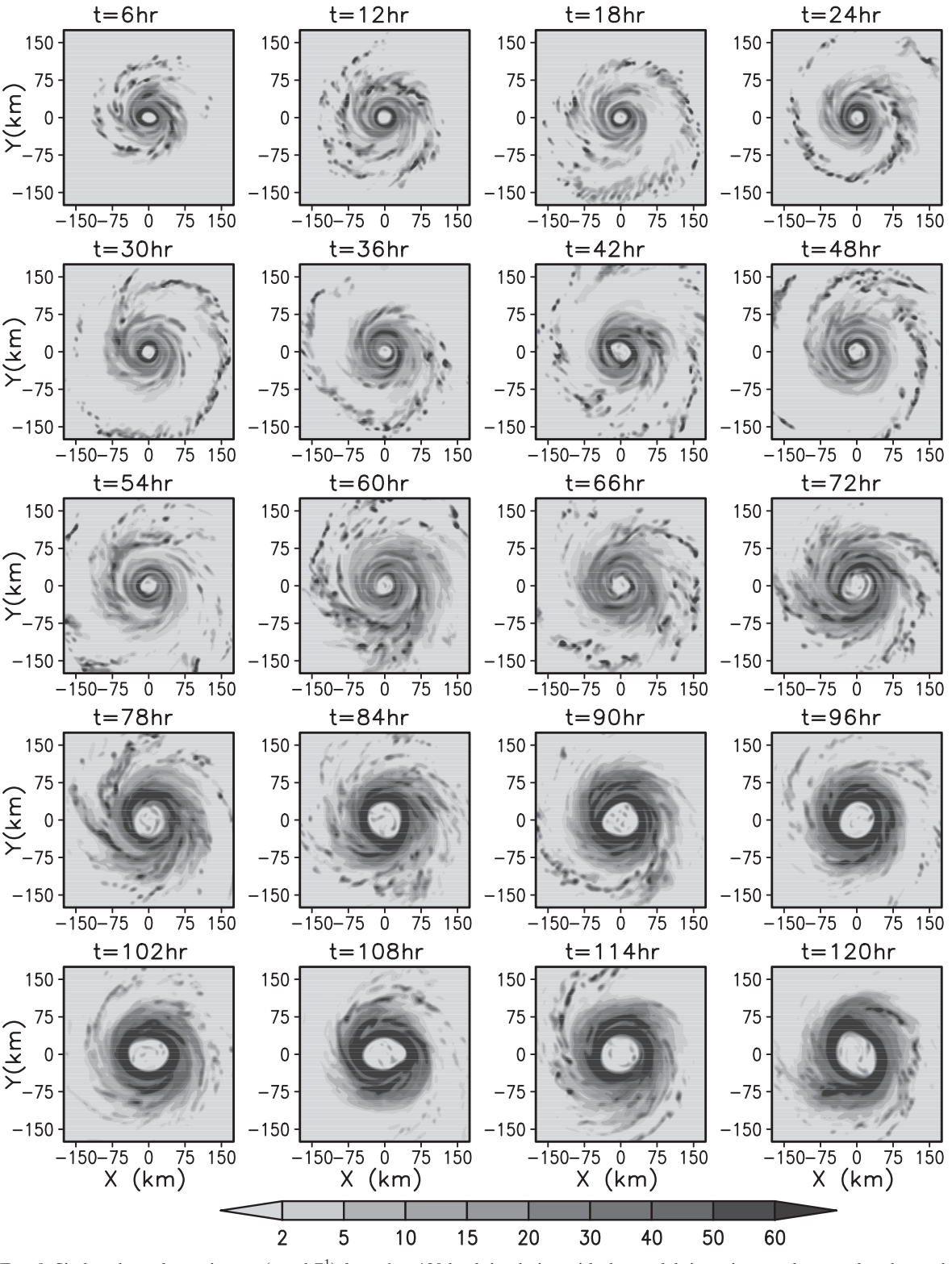

FIG. 9. Six-hourly surface rain rate (mm h^{-1}) from 6 to 120 h of simulation with the model time given at the top of each panel from experiment C80, showing the formation of the annular hurricane structure.

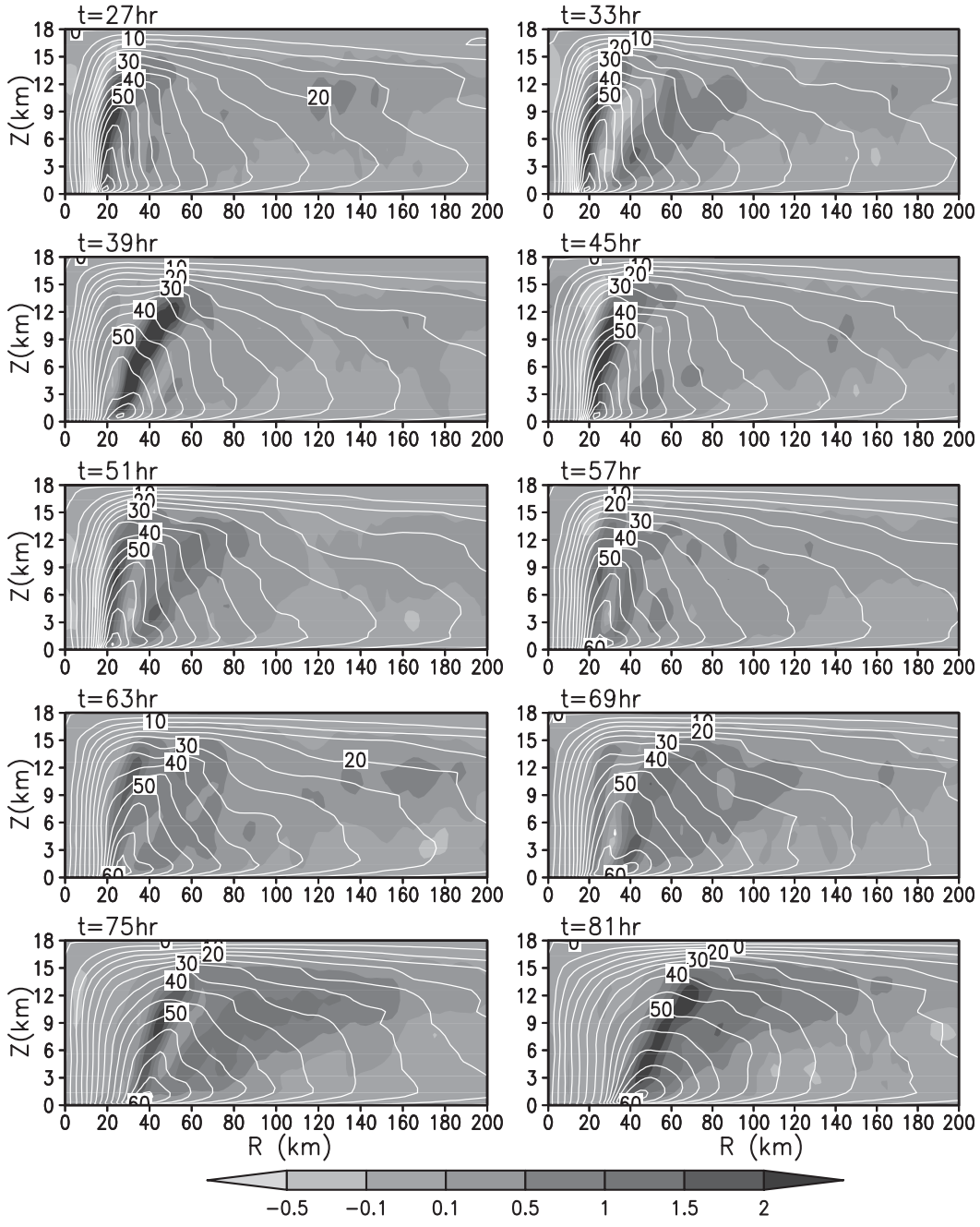

FIG. 10. Six-hourly radial–vertical structure of the azimuthal mean tangential wind (CI = 5 m s^{-1}) and vertical velocity (m s^{-1}; shading) from 27 to 81 h of simulation in experiment C80.

be a considerable PV source to the high-PV core of the storm. The numerical simulations discussed in the last section may help clarify some of the issues.

The boundary layer mass convergence into outer spiral rainbands is generally forced by diabatic heating in the rainbands due to phase changes. This is assumed previously to reduce the boundary layer mass convergence into the eyewall and thus to weaken the eyewall updraft and the storm. Because outer spiral rainbands formed randomly both in time in space, a detailed examination of their collective effect on the boundary layer inflow is not straightforward. Note that the boundary layer inflow in the simulated storms (Fig. 15d) is clearly a direct response to the total upward mass flux in the eyewall, which is driven by the internal atmospheric heating in the eyewall, as can be inferred from the net

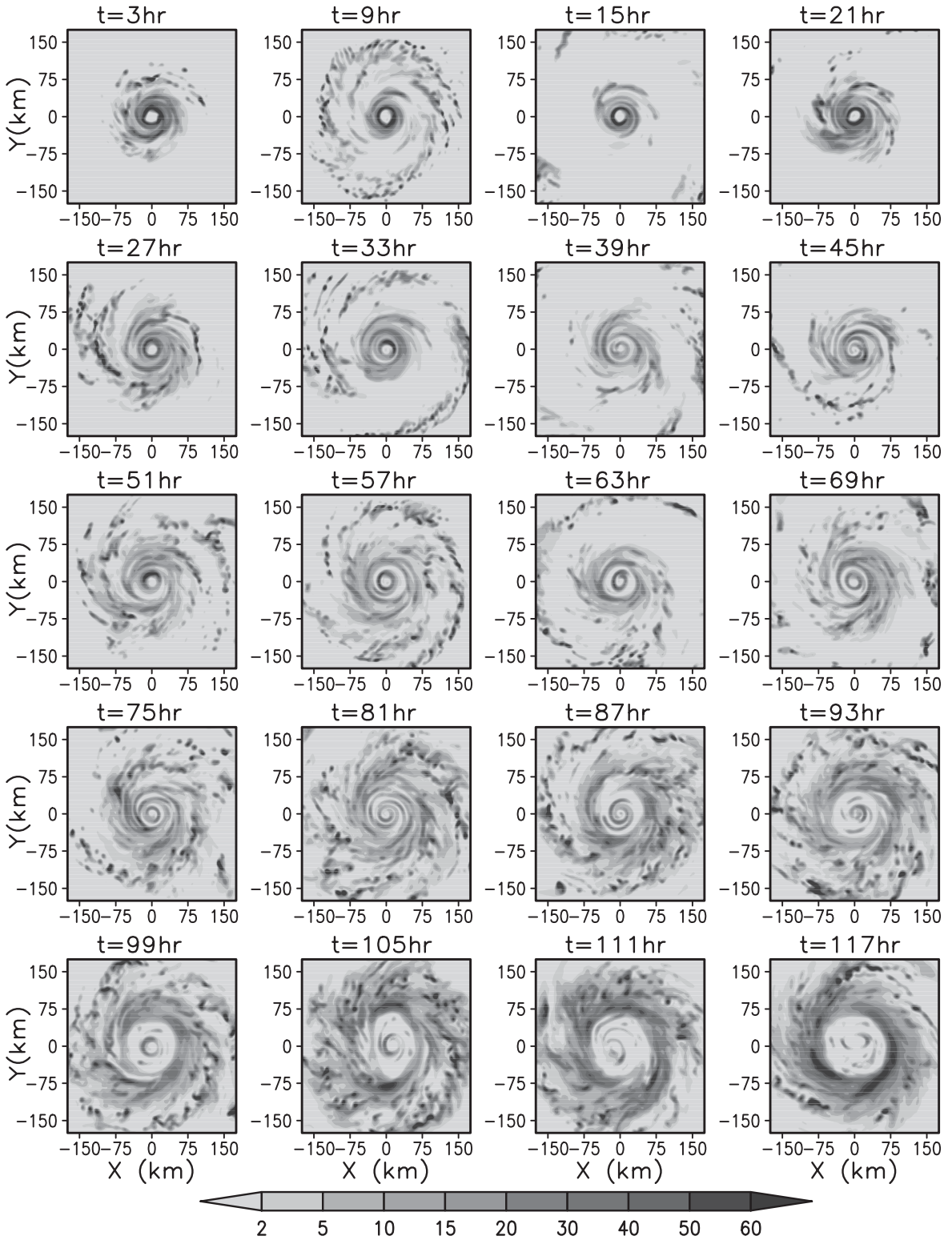

FIG. 11. Six-hourly surface rain rate (mm h^{-1}) from 3 to 117 h of simulation with the model time given at the top of each panel from experiment H110, showing the formation and life cycles of concentric eyewalls.

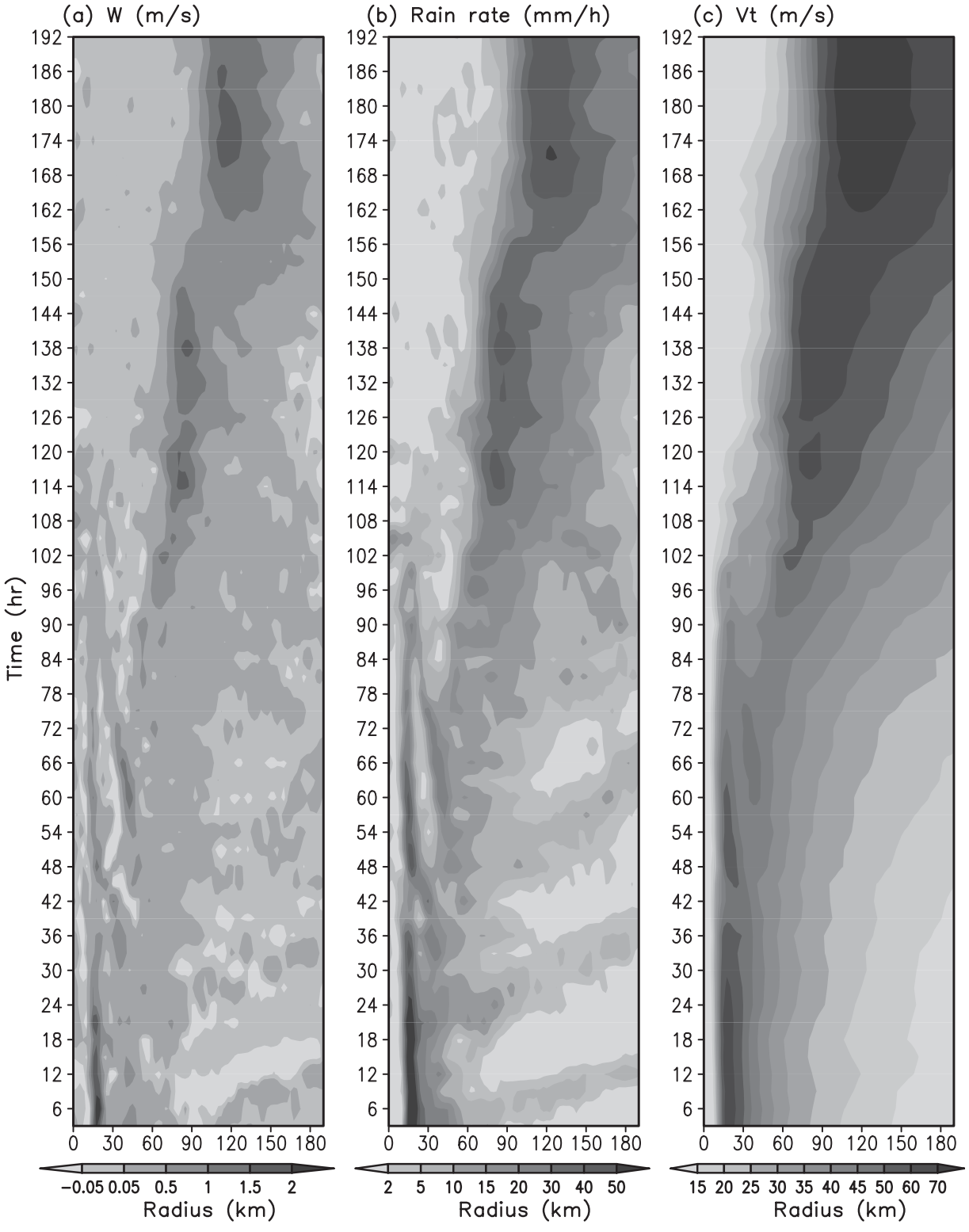

FIG. 12. Radius–time Hovmöller diagrams of (a) the azimuthal mean vertical velocity (m s^{-1}) at 3-km height, (b) surface rain rate (mm h^{-1}), and (c) tangential wind (m s^{-1}) at the lowest model level based on 3-hourly model outputs in experiment H110.

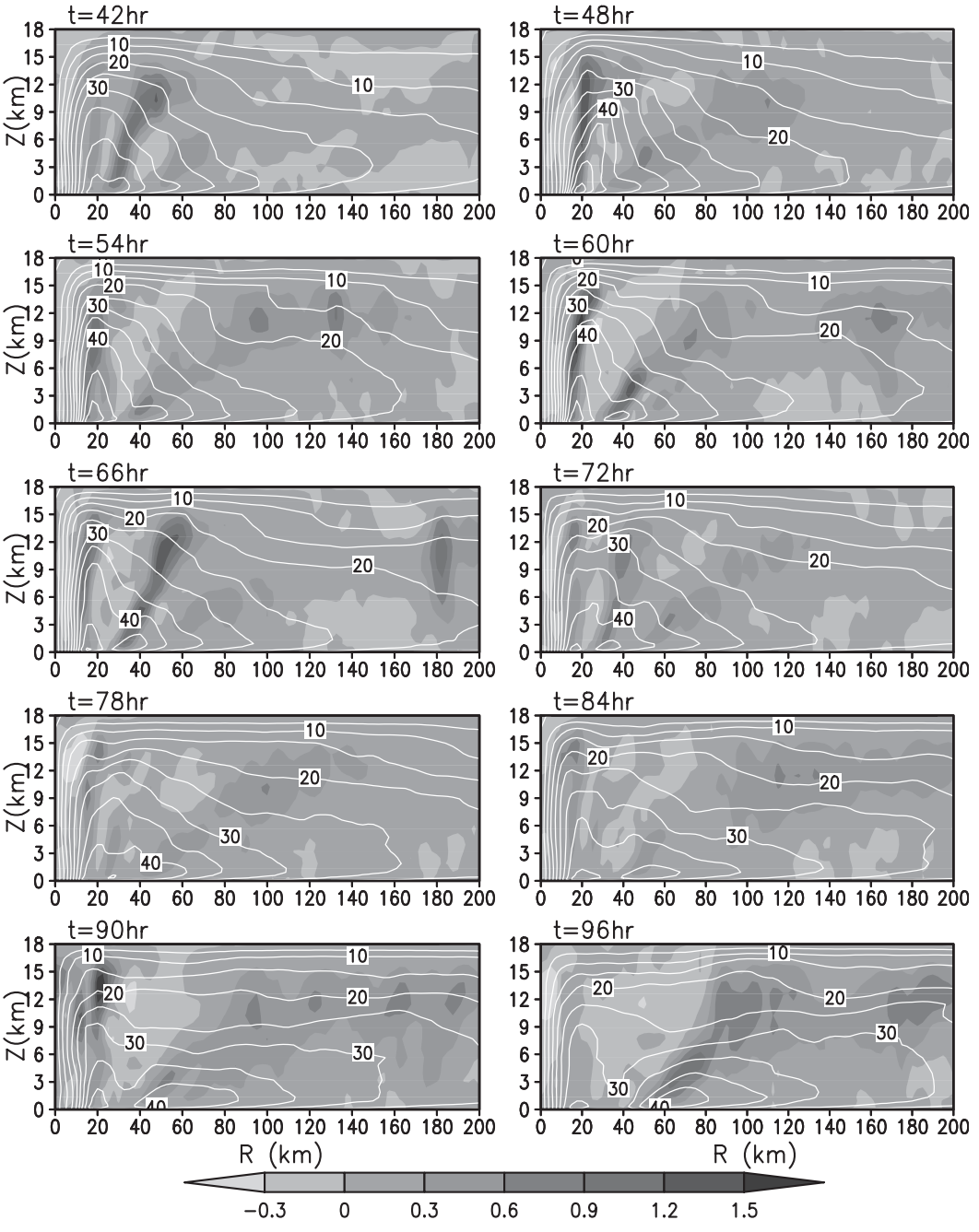

FIG. 13. Six-hourly radial–vertical structure of the azimuthal mean tangential wind (CI = 5 m s^{-1}) and vertical velocity (m s^{-1}, shading) from 42 to 96 h of simulation in experiment H110.

heat rate in the atmospheric column in Fig. 15a. Further, the boundary layer inflow is also closely correlated with the tangential wind (Fig. 15c), indicating that the boundary layer inflow can also be considered as a response to the surface friction of the cyclonic swirling flow. However, there is no close relationship between the strength of the boundary layer inflow and storm intensity in the simulated storms. Therefore, the effect of outer spiral rainbands on the storm intensity could not be simply evaluated based on the assumption of the barrier effect of the boundary layer inflow, which could also not explain the size change of the TC inner core. On the contrary, the hydrostatic adjustment mechanism discussed in the last section can clearly explain the changes in both the storm intensity and the inner-core size in the simulations. Therefore, the barrier effect of

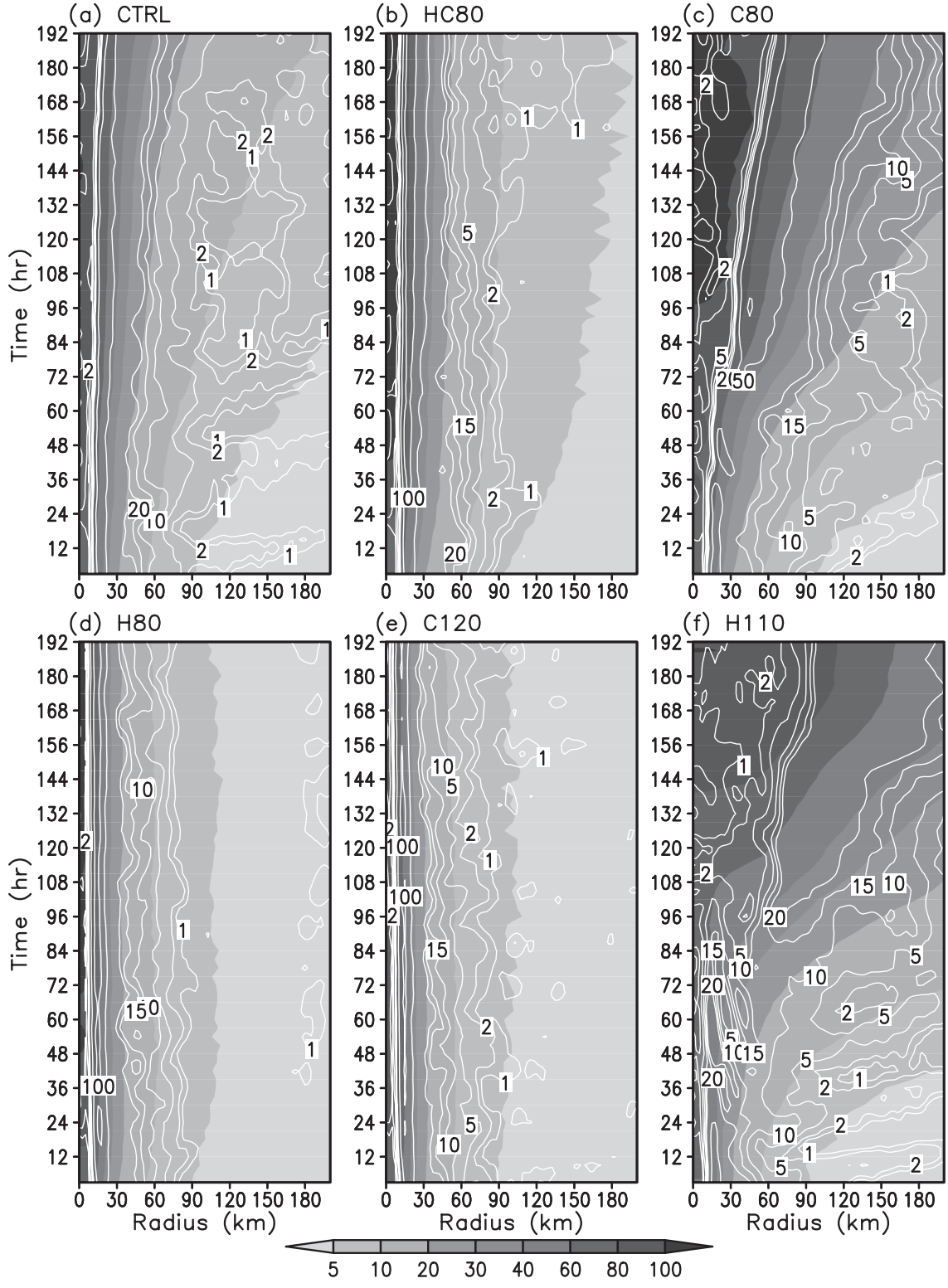

FIG. 14. Radius–time Hovmöller diagrams of the azimuthal mean surface pressure (hPa; shading) and surface rain rate (mm h^{-1}; contours with values of 1, 2, 5, 10, 20, 50, and 100 mm h^{-1}) in experiments (a) CTRL, (b) HC80, (c) C80, (d) H80, (e) C120, and (f) H110.

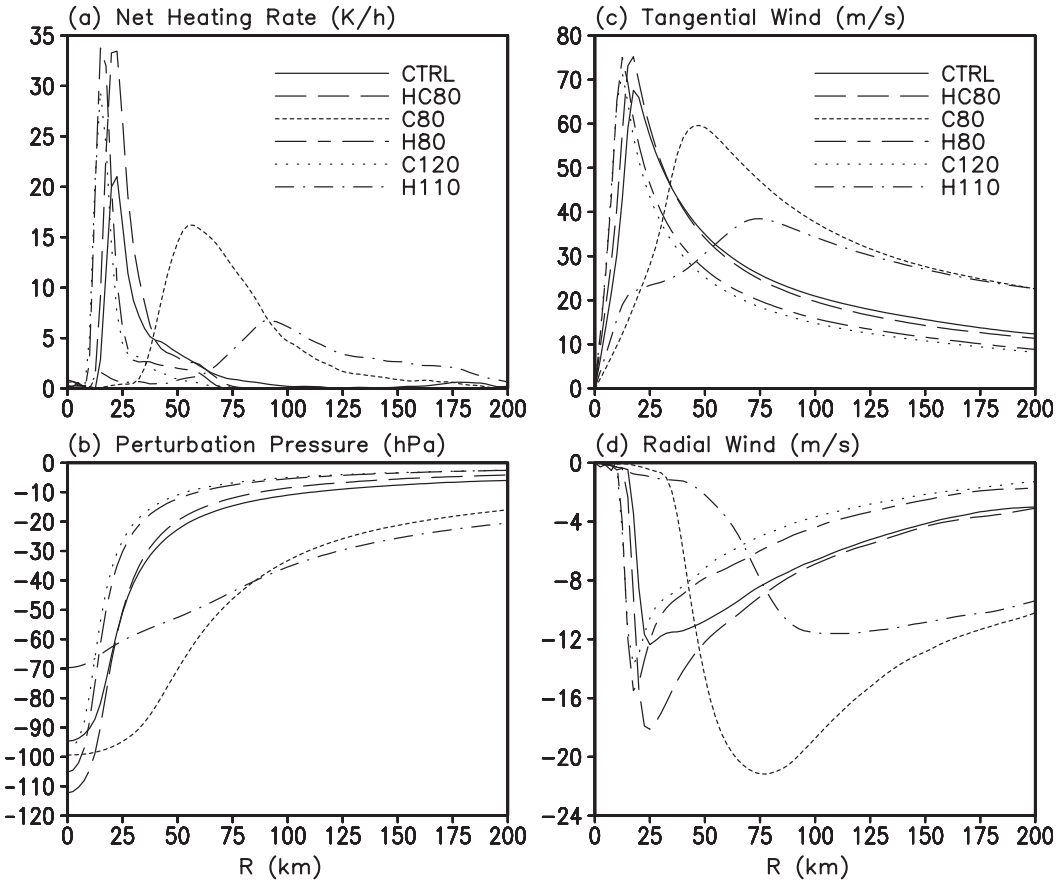

FIG. 15. Radial distributions of (a) vertically averaged net heating rate due to phase changes in the model cloud microphysics [K h^{-1}; Q^* in Eq. (2)], (b) perturbation pressure at the sea surface (hPa), (c) tangential wind (m s^{-1}) at the lowest model level, and (d) radial wind (m s^{-1}) averaged in the lowest 1 km, all averaged between 72 and 144 h of simulation in the six experiments as given in Table 1.

the boundary layer inflow associated with outer spiral rainbands needs to be evaluated with some other special strategies in future studies.

Cooling associated with phase changes in the outer spiral rainbands can generate downdrafts that could weaken the TC because they may reduce the eyewall buoyancy and convection if these air parcels are advected inward by the boundary layer inflow and entrained into the eyewall without sufficient increase in entropy extracted through sensible and latent heat from the underlying ocean. The artificial increase in the cooling rate due to phase changes outside the inner core in C120 results in a more intense storm with a more compact inner-core structure, indicating that cooling in outer spiral rainbands does not weaken a TC. This is equivalent to and thus consistent with the reduced heating in H80, which also results in a more intense and more compact storm than CTRL. Note that because in both H80 and C120 the outer spiral rainbands were largely suppressed in the simulations after some initial adjustments, the increase in net cooling in C120 or the reduction of net heating in H80 was negligible outside the inner core (Fig. 15a). However, the net heating in the atmospheric column in CTRL in comparison with little heating in C120 and H80 outside the inner core indicates that a relative cooling in both C120 and H80 explains the stronger and more compact storms. Because the net heating outside the inner core is associated with the outer spiral rainbands in CTRL, it is suggested that any cooling that can offset the heating effect associated with outer spiral rainbands may contribute positively to the storm intensity and the compact inner-core structure. Because downdrafts in outer spiral rainbands have a net cooling effect outside the inner core in the boundary layer (Barnes et al. 1983; Powell 1990a,b), the above results imply that downdrafts in outer spiral rainbands might not weaken a TC, whereas they could be crucial to the maintenance of a strong TC with a relatively compact inner-core structure. Consistently, with the cooling rate reduced outside the inner core in

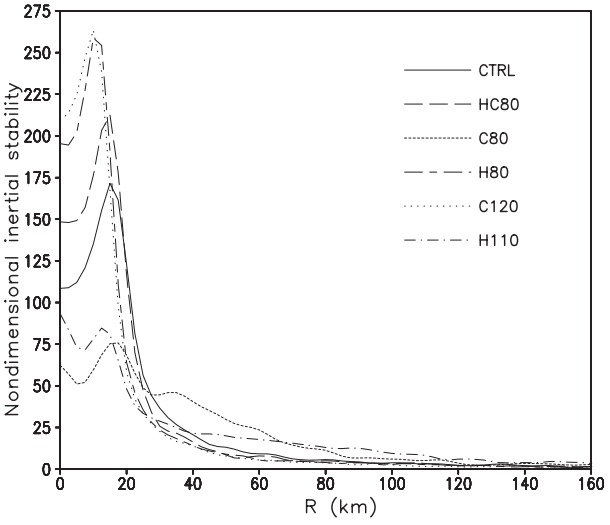

FIG. 16. Inertial stability parameter normalized by the local Coriolis parameter, namely, $I = \sqrt{(f_0 + 2V/r)[f_0 + \partial rV/(r\partial r)]}/f_0$, where f_0 is the Coriolis parameter at the center of the model TC, V the tangential wind, and r the radial distance from the TC center, averaged over the 192-h simulations with 3-hourly outputs from the six experiments as given in Table 1.

C80, the model TC had a much larger inner-core size with a weaker intensity, opposite to the case in C120 (Figs. 4,8, 14, and 15).

Bister and Emanuel (1997) and Bister (2001) found that intensification of their model TC was earlier and faster when surface sensible and latent heat fluxes outside the inner core were suppressed because this suppressed convection in the outer region. They explained that the response of the model TC to convection outside the inner core would increase the tangential wind in the outer region and decrease it in most of the inner region in the boundary layer. These effects delayed and slowed intensification of the model storm. With both the heating and cooling rates reduced outside the inner core in HC80, the storm did not develop strong outer spiral rainbands and reached almost the same intensity as in H80, in which only the heating rate was reduced. Storms in both HC80 and H80 are considerably stronger than the storm in CTRL (Fig. 5). In a supplementary experiment in which both the heating and cooling rates from the cloud microphysics were reduced to zero outside the inner core, the storm reached an intensity very similar to that in HC80 without active outer spiral rainbands (not shown). Therefore, overall outer spiral rainbands weaken a TC.

The PV source hypothesis by May and Holland (1999) has not been explicitly examined in this study. Because outer spiral rainbands are not very active in these idealized model simulations, any PV generation due to the vertical heating gradient in outer rainbands would mainly increase the tangential winds locally outside the rainbands (Hence and Houze 2008) and would tend to increase the storm size. However, the inward propagation of inner spiral rainbands may bring cyclonic PV anomalies to the eyewall and contribute to the formation of the annular hurricane, as in C80. Large PV generation in strong outer spiral rainbands may contribute to the formation of a concentric eyewall as proposed by Kuo et al. (2004). This may weaken a TC, as was the case in H110. Thus, instead of strengthening a TC as hypothesized by May and Holland (1999), PV generation in the outer spiral rainbands could contribute to the formation of a concentric eyewall and thus would weaken but increase the size of the storm.

With the heating/cooling rate associated with cloud microphysics artificially modified in the sensitivity experiments discussed in the last section, several structure changes—such as the formation of an annular hurricane, the development of a concentric eyewall, and the size changes—were simulated that have similar characteristics to previous studies (Willoughby et al. 1984; Wang 2002c; Zhu and Zhang 2006; McFarquhar et al. 2006; Sawada and Iwasaki 2007). Because the internal atmospheric heating/cooling outside the inner core depends strongly on the relative humidity, TC structure and intensity changes can be expected to be sensitive to the relative humidity in the near-core environment.

One implication from these experiments is that a TC with a large size is unlikely to develop in a relatively dry environment because cooling due to evaporation of cloud droplets and rainwater and melting of snow and graupel would be large and heating due to condensation, freezing, and deposition would be small. This implication is consistent with the relatively small size of TCs that affect the Hawaiian region, which generally exist in the shallow moist layer in the trade wind regime of the subtropical central Pacific. The smaller TCs in the North Atlantic could be partly due to the dry Saharan Air Layer (SAL; Dunion and Velden 2004; Jones et al. 2007). By contrast, TCs in the Pacific Northwest are generally large because they usually form and develop in the moisture-rich monsoon trough. The large background vorticity in the western Pacific monsoon trough may also contribute to the large TCs in the region (G. J. Holland 2007, personal communication). The relative importance of the environmental relative humidity and the background vorticity will be a topic for a future study with well-designed numerical experiments.

The storm in C80 developed an annular hurricane structure after only 3–4 days of simulation (after a 2-day spinup) compared with the 9–10 days in Wang (2008b). Further examination of the simulation in Wang (2008b) indicates that the moistening of the near-core environment is an important precondition to the formation of

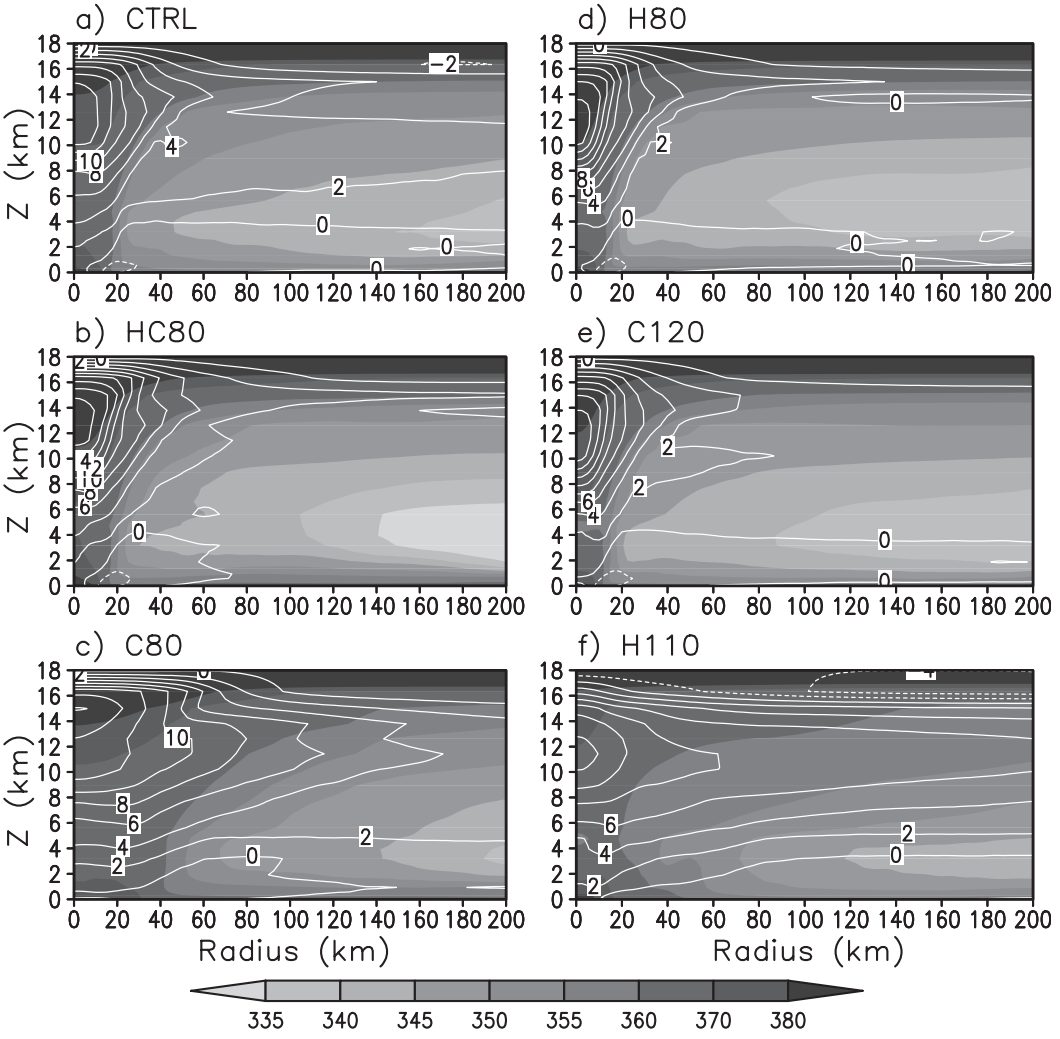

FIG. 17. Radial–vertical distributions of azimuthal mean temperature anomalies (CI = 2 K) and equivalent potential temperature (K; shading) averaged between 72 and 96 h of integration from experiments (a) CTRL, (b) HC80, (c) C80, (d) H80, (e) C120, and (f) H110.

the annular hurricane (not shown). Such moistening was achieved by active convection outside the inner-core region. A moister near-core environment reduces cooling due to evaporation of rain and melting of snow and graupel and increases heating due to condensation and deposition in the outer spiral rainbands and anvil clouds, both favoring the formation of the annular hurricane as in C80. Because the moistening in Wang (2008b) took a relatively long time, artificially reduced cooling outside the inner core in C80 allowed the annular hurricane to develop much earlier. In an additional experiment, in which a higher relative humidity than in CTRL was specified in the initial sounding, the annular hurricane developed in less than 5 days (not shown). A comparison of the near-core environmental relative humidity between annular hurricanes and regular hurricanes from observations will provide more evidence with regard to the above finding.

The result from experiment H110 indicates the importance of heating in outer spiral rainbands to the formation of the concentric eyewall in TCs. Heating in outer spiral rainbands is sensitive to the relative humidity in the near-core environment as well. Nong and Emanuel (2003) showed that simulation of concentric eyewall formation is very sensitive to the initial environmental relative humidity in their simple TC model. In an experiment with environmental relative humidity increased to 90% in the troposphere, the concentric eyewall cycle was simulated on an *f* plane in TCM4 (not shown), consistent with the results of Nong and Emanuel (2003). Thus, a deep moist layer in the near-core environment of a TC favors the formation of not only

annular hurricanes but also concentric eyewalls. Hawkins and Helveston (2004) found that about 80% of the intense TCs over the western North Pacific develop a concentric eyewall in their lifetime compared to only about 40% of the intense TCs in the North Atlantic. This contrast may result in part from the difference in large-scale moisture fields in the two basins as mentioned above. This could be another topic for a future observational study.

6. Conclusions

It has been speculated for a long time that outer spiral rainbands could have a significant effect on tropical cyclone structure and intensity. However, their effect has not been evaluated in a measurable, explicit way because of the highly nonlinear nature of the physical processes involved. In this study, the effect of outer spiral rainbands on the structure and intensity of tropical cyclones was evaluated based on a series of sensitivity experiments using the cloud-resolving tropical cyclone model TCM4. The working hypothesis is based on the fact that the outer spiral rainbands are driven mainly by diabatic heating due to phase changes in the rainbands. Therefore, the effect of outer spiral rainbands on tropical cyclone intensity and structure was investigated by artificially modifying the heating/cooling rate calculated from the cloud microphysics in the model. The effect of diabatic heating due to phase changes in outer spiral rainbands on the overall storm structure and intensity is thought to be mostly the result of hydrostatic adjustment; that is, internal atmospheric heating (cooling) would tend to decrease (increase) surface pressure underneath the column. The actual change in surface pressure due to heating in the outer spiral rainbands is significant on the inward side of the rainbands near the inner core where the inertial stability is high but is relatively small outside the rainbands in the far field, where the inertial stability is low and internal atmospheric heating is mostly lost to gravity wave radiation and little heat is left to warm the atmospheric column and lower the local surface pressure (Hack and Schubert 1982; Shapiro and Willoughby 1982). As a result, heating in outer spiral rainbands, on the one hand, would reduce the horizontal pressure gradient across the radius of maximum wind and thus the storm intensity in terms of the maximum wind in the lower troposphere and, on the other hand, would increase the inner-core size of the storm.

The results show that cooling due to evaporation of rain and melting of snow and graupel in the outer spiral rainbands is important to both the intensity of the tropical cyclone and the maintenance of a relatively compact storm structure. Heating in the outer spiral rainbands decreases intensity but increases the inner-core size. Overall, the presence of strong outer spiral rainbands limits the intensity of tropical cyclones. Because heating/cooling outside the inner core depends strongly on the relative humidity in the near-core environment, the results imply that the structure and intensity changes of a tropical cyclone could be very sensitive to its environmental relative humidity. Results from this study suggest that the deep moist layer in the near-core environment can modify the heating/cooling rate due to phase changes in the outer spiral rainbands and may favor the development of large tropical cyclones, annular hurricane structure, and concentric eyewalls; conversely, a relatively dry environment may favor small, compact tropical cyclones and is unfavorable to the formation of annular hurricanes or concentric eyewalls. Future observational studies should be carried out to confirm these implications from the present idealized model simulations.

Acknowledgments. The author is grateful to Prof. Russ Elsberry and two anonymous reviewers for their helpful comments and to Dr. Gisela Speidel for her help in improving the representations of the manuscript. This study has been supported by NSF Grants ATM-0427128 and ATM-0754039 and ONR Grant 00014-06-10303. Additional support has been provided by JAMSTEC, NASA, and NOAA through their sponsorships of the International Pacific Research Center (IPRC) in the School of Ocean and Earth Science and Technology (SOEST) at the University of Hawaii.

REFERENCES

Anthes, R. A., 1982: *Tropical Cyclones: Their Evolution, Structure and Effects. Meteor. Monogr.,* No. 41, Amer. Meteor. Soc., 208 pp.

Barnes, G. M., E. J. Zipser, D. Jorgensen, and F. Marks Jr., 1983: Mesoscale and convective structure of a hurricane rainband. *J. Atmos. Sci.,* **40,** 2125–2137.

Bister, M., 2001: Effect of peripheral convection on tropical cyclone formation. *J. Atmos. Sci.,* **58,** 3463–3476.

——, and K. A. Emanuel, 1997: The genesis of Hurricane Guillermo: TEXMEX analyses and a modeling study. *Mon. Wea. Rev.,* **125,** 2662–2682.

Chen, Y., and M. K. Yau, 2001: Spiral bands in a simulated hurricane. Part I: Vortex Rossby wave verification. *J. Atmos. Sci.,* **58,** 2128–2145.

Chow, K. C., K. L. Chan, and A. K. H. Lau, 2002: Generation of moving spiral bands in tropical cyclones. *J. Atmos. Sci.,* **59,** 2930–2950.

Diercks, J. W., and R. A. Anthes, 1976: Diagnostic studies of spiral rainbands in a nonlinear hurricane model. *J. Atmos. Sci.,* **33,** 959–975.

Dunion, J. P., and C. S. Velden, 2004: The impact of the Saharan air layer on Atlantic tropical cyclone activity. *Bull. Amer. Meteor. Soc.,* **85,** 353–365.

Durran, D. R., and J. B. Klemp, 1983: A compressible model for the simulation of moist mountain waves. *Mon. Wea. Rev.,* **111,** 2341–2361.

Fairall, C. W., E. F. Bradley, J. E. Hare, A. A. Grachev, and J. B. Edson, 2003: Bulk parameterization of air–sea fluxes: Updates and verification for the COARE algorithm. *J. Climate,* **16,** 571–591.

Franklin, C. N., G. J. Holland, and P. T. May, 2005: Sensitivity of tropical cyclone rainbands to ice-phase microphysics. *Mon. Wea. Rev.,* **133,** 2473–2493.

Gray, W. M., E. Ruprecht, and R. Phelps, 1975: Relative humidity in tropical weather systems. *Mon. Wea. Rev.,* **103,** 685–690.

Hack, J., and W. H. Schubert, 1986: Nonlinear response of atmospheric vortices to heating by organized cumulus convection. *J. Atmos. Sci.,* **43,** 1559–1573.

Hawkins, J. D., and M. Helveston, 2004: Tropical cyclone multiple eyewall characteristics. Preprints, *26th Conf. on Hurricanes and Tropical Meteorology,* Miami, FL, Amer. Meteor. Soc., P1.7. [Available online at http://ams.confex.com/ams/26HURR/techprogram/paper_76084.htm.]

Hence, D. A., and R. A. Houze Jr., 2008: Kinematic structure of convective-scale elements in the rainbands of Hurricane Katrina and Rita (2005). *J. Geophys. Res.,* **113,** D15108, doi:10.1029/2007JD009429.

Holland, G. J., 1997: The maximum potential intensity of tropical cyclones. *J. Atmos. Sci.,* **54,** 2519–2541.

Jones, T. A., D. J. Cecil, and J. P. Dunion, 2007: The environmental and inner-core conditions governing intensity of Hurricane Erin (2001). *Wea. Forecasting,* **22,** 708–725.

Kimball, S. K., and F. C. Dougherty, 2006: The sensitivity of idealized hurricane structure and development to the distribution of vertical levels in MM5. *Mon. Wea. Rev.,* **134,** 1987–2008.

Knaff, J. A., J. P. Kossin, and M. DeMaria, 2003: Annular hurricanes. *Wea. Forecasting,* **18,** 204–223.

Kossin, J. P., and W. H. Schubert, 2001: Mesovortices, polygonal flow patterns, and rapid falls in hurricane-like vortices. *J. Atmos. Sci.,* **58,** 2196–2209.

Kuo, H.-C., R. T. Williams, and J.-H. Chen, 1999: A possible mechanism for the eye rotation of typhoon Herb. *J. Atmos. Sci.,* **56,** 1659–1673.

——, L.-Y. Lin, C.-P. Chang, and R. T. Williams, 2004: The formation of concentric vorticity structures in typhoons. *J. Atmos. Sci.,* **61,** 2722–2734.

Kurihara, Y., 1976: On the development of spiral bands in a tropical cyclone. *J. Atmos. Sci.,* **33,** 940–958.

Langland, R. H., and C.-S. Liou, 1996: Implementation of an E–ε parameterization of vertical subgrid-scale mixing in a regional model. *Mon. Wea. Rev.,* **124,** 905–918.

May, P. T., and G. J. Holland, 1999: The role of potential vorticity generation in tropical cyclone rainbands. *J. Atmos. Sci.,* **56,** 1224–1228.

McFarquhar, G. M., H. N. Zhang, G. Heymsfield, J. B. Halverson, R. Hood, J. Dudhia, and F. Marks Jr., 2006: Factors affecting the evolution of Hurricane Erin (2001) and the distributions of hydrometeors: Role of microphysical processes. *J. Atmos. Sci.,* **63,** 127–150.

Montgomery, M. T., and R. J. Kallenbach, 1997: A theory for vortex Rossby-waves and its application to spiral bands and intensity changes in hurricanes. *Quart. J. Roy. Meteor. Soc.,* **123,** 435–465.

Nolan, D. S., and M. T. Montgomery, 2002: Nonhydrostatic, three-dimensional perturbations to balanced, hurricane-like vortices. Part I: Linearized formulation, stability, and evolution. *J. Atmos. Sci.,* **59,** 2989–3020.

——, and L. D. Grasso, 2003: Nonhydrostatic, three-dimensional perturbations to balanced, hurricane-like vortices. Part II: Symmetric response and nonlinear simulations. *J. Atmos. Sci.,* **60,** 2717–2745.

Nong, S.-Y., and K. A. Emanuel, 2003: A numerical study of the genesis of concentric eyewalls in hurricanes. *Quart. J. Roy. Meteor. Soc.,* **129,** 3323–3338.

Persing, J., and M. T. Montgomery, 2005: Is environmental CAPE important in the determination of maximum possible hurricane intensity? *J. Atmos. Sci.,* **62,** 542–550.

Powell, M. D., 1990a: Boundary layer structure and dynamics in outer hurricane rainbands. Part I: Mesoscale rainfall and kinematic structure. *Mon. Wea. Rev.,* **118,** 891–917.

——, 1990b: Boundary layer structure and dynamics in outer hurricane rainbands. Part II: Downdraft modification and mixed layer recovery. *Mon. Wea. Rev.,* **118,** 918–938.

Rotunno, R., and K. Emanuel, 1987: An air–sea interaction theory for tropical cyclones. Part II: Evolutionary study using a nonhydrostatic axisymmetric model. *J. Atmos. Sci.,* **44,** 542–561.

Rozoff, C. M., W. H. Schubert, and B. D. McNoldy, 2006: Rapid filamentation zones in intense tropical cyclones. *J. Atmos. Sci.,* **63,** 325–340.

Sawada, M., and T. Iwasaki, 2007: Impacts of ice phase processes on tropical cyclone development. *J. Meteor. Soc. Japan,* **85,** 479–494.

Schecter, D. A., and M. T. Montgomery, 2004: Damping and pumping of a vortex Rossby wave in a monotonic cyclone: Critical layer stirring versus inertia–buoyancy wave emission. *Phys. Fluids,* **16,** 1334–1348.

——, and ——, 2006: Conditions that inhibit the spontaneous radiation of spiral inertia–gravity waves from an intense mesoscale cyclone. *J. Atmos. Sci.,* **63,** 435–456.

——, and ——, 2007: Waves in a cloudy vortex. *J. Atmos. Sci.,* **64,** 314–337.

Schubert, W. H., M. T. Montgomery, R. K. Taft, T. A. Guinn, S. R. Fulton, J. P. Kossin, and J. P. Edwards, 1999: Polygonal eyewalls, asymmetric eye contraction, and potential vorticity mixing in hurricanes. *J. Atmos. Sci.,* **56,** 1197–1223.

Shapiro, L. J., and H. E. Willoughby, 1982: The response of balanced hurricanes to local sources of heat and momentum. *J. Atmos. Sci.,* **39,** 378–394.

Wang, Y., 1996: On the forward-in-time upstream advection scheme for non-uniform and time-dependent flow. *Meteor. Atmos. Phys.,* **61,** 27–38.

——, 2001: An explicit simulation of tropical cyclones with a triply nested movable mesh primitive equation model: TCM3. Part I: Model description and control experiment. *Mon. Wea. Rev.,* **129,** 1370–1394.

——, 2002a: Vortex Rossby waves in a numerically simulated tropical cyclone. Part I: Overall structure, potential vorticity, and kinetic energy budgets. *J. Atmos. Sci.,* **59,** 1213–1238.

——, 2002b: Vortex Rossby waves in a numerically simulated tropical cyclone. Part II: The role in tropical cyclone structure and intensity changes. *J. Atmos. Sci.,* **59,** 1239–1262.

——, 2002c: An explicit simulation of tropical cyclones with a triply nested movable mesh primitive equation model: TCM3. Part II: Model refinements and sensitivity to cloud microphysics parameterization. *Mon. Wea. Rev.,* **130,** 3022–3036.

——, 2007: A multiply nested, movable mesh, fully compressible, nonhydrostatic tropical cyclone model—TCM4: Model description and development of asymmetries without explicit asymmetric forcing. *Meteor. Atmos. Phys.,* **97,** 93–116.

——, 2008a: Rapid filamentation zone in a numerically simulated tropical cyclone. *J. Atmos. Sci.,* **65,** 1158–1181.

——, 2008b: Structure and formation of an annular hurricane simulated in a fully compressible, nonhydrostatic model—TCM4. *J. Atmos. Sci.,* **65,** 1505–1527.

——, and C.-C. Wu, 2004: Current understanding of tropical cyclone structure and intensity changes–A review. *Meteor. Atmos. Phys.,* **87,** 257–278.

Wicker, L. J., and W. C. Skamarock, 2002: Time-splitting methods for elastic models using forward time schemes. *Mon. Wea. Rev.,* **130,** 2088–2097.

Willoughby, H. E., 1978: A possible mechanism for the formation of hurricane rainbands. *J. Atmos. Sci.,* **35,** 838–848.

——, J. A. Clos, and M. G. Shoreibah, 1982: Concentric eye walls, secondary wind maxima and the evolution of the hurricane vortex. *J. Atmos. Sci.,* **39,** 395–411.

——, H.-L. Jin, S. J. Lord, and J. M. Piotrowicz, 1984: Hurricane structure and evolution as simulated by an axisymmetric, nonhydrostatic numerical model. *J. Atmos. Sci.,* **41,** 1169–1186.

Zhang, D.-L., and X. Wang, 2003: Dependence of hurricane intensity and structures on vertical resolution and time-step size. *Adv. Atmos. Sci.,* **20,** 711–725.

Zhu, T., and D.-L. Zhang, 2006: A numerical simulation of Hurricane Bonnie (1998). Part II: Sensitivity to varying cloud microphysical processes. *J. Atmos. Sci.,* **63,** 109–126.